Journal of South American Earth Sciences 114 (2022) 103688

Contents lists available at ScienceDirect

Journal of South American Earth Sciences

journal homepage: www.elsevier.com/locate/jsames

A multi-method approach to constrain the age of eruption and post-depositional processes in a Lower Jurassic ignimbrite from the Marifil Volcanic Complex, eastern North Patagonian Massif

Santiago N. González [a,b,*], Gerson A. Greco [a,b], Antonella Galetto [c], Sofia Bordes [d], Miguel A. S. Basei [e], Martín N. Parada [a,b], Raúl E. Giacosa [a,f], M. Josefina Pons [a,b]

[a] Universidad Nacional de Río Negro, Instituto de Investigación en Paleobiología y Geología, Río Negro, Argentina
[b] IIPG, UNRN - Consejo Nacional de Investigaciones Científicas y Tecnológicas (CONICET). Av. Roca 1242, (R8332EXZ) General Roca, Río Negro, Argentina
[c] CONICET-IDEAN, Universidad de Buenos Aires, Ciudad Universitaria, C1428EHA, Buenos Aires, Argentina
[d] La.Te. Andes SA (GEOMAP-CONICET), Las Moreras 510, 4401, Vaqueros, Salta, Argentina
[e] Centro de Pesquisas em Geocronologia e Geoquímica Isotópica (CPGeo) - Universidad de San Pablo, Brazil
[f] Servicio Geológico Minero Argentino (SEGEMAR), delegación General Roca, Argentina

ARTICLE INFO

Keywords:
Jurassic
Patagonia
Volcanism
Chon aike
U–Pb
Fission-track
Apatite
Zircon
Low-temperature thermochronology

ABSTRACT

In the eastern North Patagonian Massif, the Marifil Volcanic Complex corresponds to an Early Jurassic magmatic event. In this study, we evaluate new geochronological and thermochronological data obtained from an ignimbrite of the complex. U–Pb zircon ages from the pumice fraction reveal a Concordia age of 184.4 ± 1.1 Ma. Conversely, U–Pb zircon ages from the whole-rock sample evidence a Concordia age of 190.4 ± 0.6 Ma. Fission track techniques were applied on the same whole-rock sample. Zircon fission track performed on the same zircon-crystals dated by U–Pb yielded an age of 172.5 ± 8.1 Ma, while apatite fission track evidenced a cooling age of 179.1 ± 13.5 Ma. Apatite and zircon crystals describe uniform morphologies with unaltered euhedral to subhedral grains and well-developed crystalline forms. The results suggest that the age of eruption and deposition of the ignimbrite is better explained by the pumice zircon age rather than the whole-rock zircon age. Inherited grain-ages and petrographic evidence support provenance from older, probably cogenetic, magmatic products. Fission track ages reflect a post-depositional process probably related to diagenetic mineral changes.

1. Introduction

During volcanic eruptions, lava, rock fragments, and gases are ejected to the Earth's atmosphere and deposited on the surface. Within those materials, crystals formed in the magmatic reservoir can be found. A significant uncertainty resides when trying to establish how distant in time is the age of eruption from the age of crystallization of those crystals. The reliability of isotopic ages to constrain volcanic events depend, among other factors, on the applied dating method and the characteristics of the geological material under study. Nowadays, the U–Pb isotopic dating method, commonly applied on zircon crystals, allows performing punctual analyses in single grains (SHRIMP, LA-ICP-MS, among others). By applying this method on a spot of an entire grain and by reproducing it on a large number of crystals of the same sample, the quality, and precision of the outcoming result increase. Moreover, this particular methodology also allows to date multiple events in a single crystal grain (Simon et al., 2008; Storm et al., 2011; Fornelli et al., 2014; Cooper, 2015). The application of crystallization ages in terms of more specific priors, in addition to thermochronological data, is essential to present a well-constrained thermal history with a better focused time-temperature range (Gallagher, 2012).

In Patagonia, southern south America (Fig. 1), the Chon Aike Silicic Large Igneous Province includes a large volume of mostly acidic volcanic rocks, widely distributed (Pankhurst et al., 2011 and references therein). The Marifil Volcanic Complex (Malvicini and Llambías, 1974; Cortés, 1981; Busteros et al., 1998) belongs to the Chon Aike Province (Pankhurt et al., 1998, 2000) and has been included in the eastern domain of the Jurassic magmatism of the North Patagonian Massif (Zaffarana et al., 2020). It was considered as the first volcanic episode of the igneous province that occurred between 188 and 178 Ma (Pankhurst

* Corresponding author. Universidad Nacional de Río Negro. Instituto de Investigación en Paleobiología y Geología, Río Negro, Argentina.
E-mail address: sgonzalez@unrn.edu.ar (S.N. González).

https://doi.org/10.1016/j.jsames.2021.103688
Received 16 August 2021; Received in revised form 3 December 2021; Accepted 16 December 2021
Available online 1 January 2022

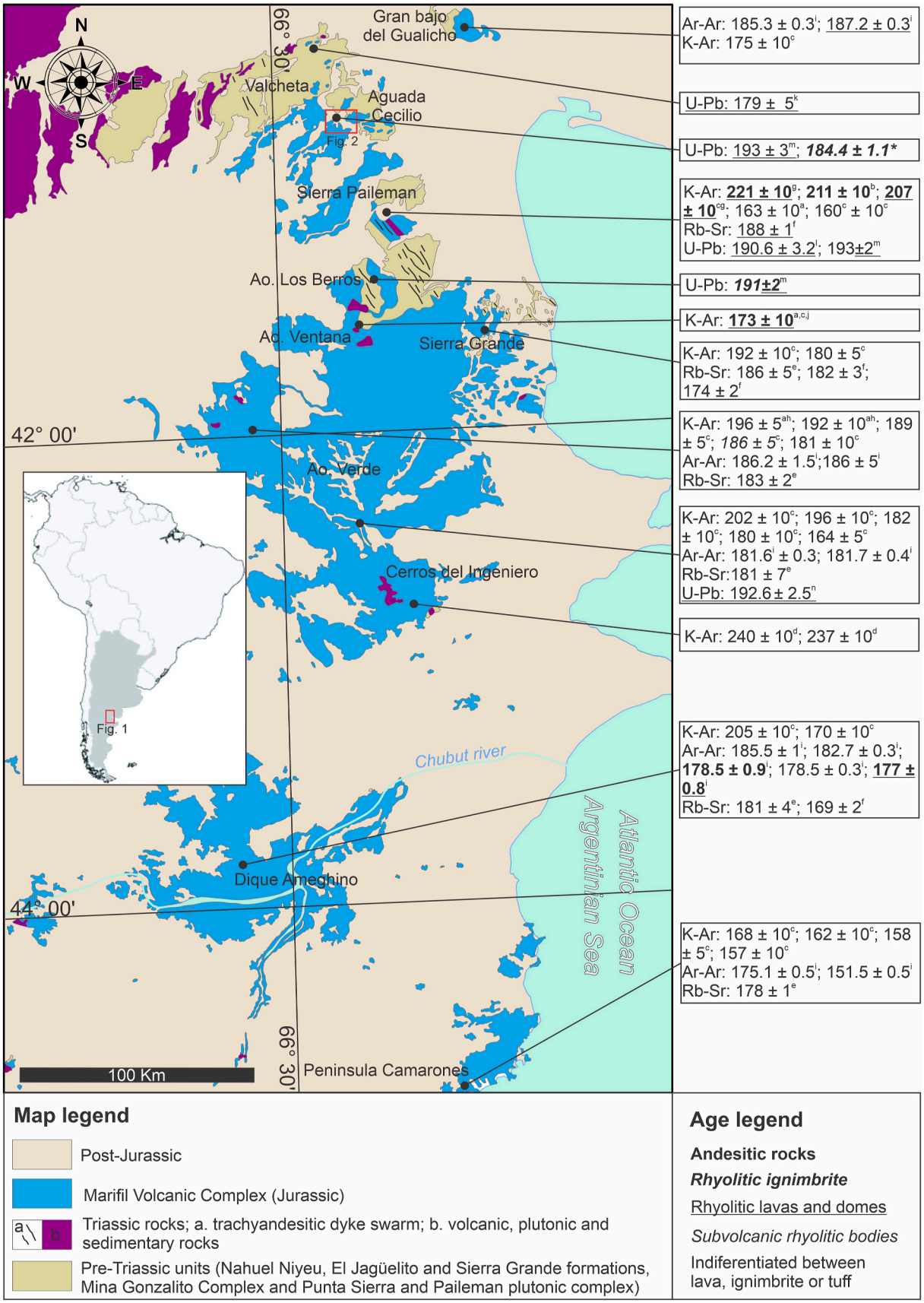

Fig. 1. Outcrops of the Marifil Volcanic Complex in the eastern North Patagonian Massif (eastern domain in Zaffarana et al. 2020) showing known radiometric ages for each one. References a: Núñez et al. (1975); b: Valles (1978); c: Cortés (1981); d: Haller (1981); e: Rapela and Pankhurst (1993); f: Pankhurst and Rapela (1995); g: Genovese (1995); h: Busteros et al. (1998); i: Féraud et al. (1999); j: Franchi et al. (2001); k: Chernicoff et al. (2017); l: Strazzere et al. (2017); m: Strazzere et al. (2019); n: Pavón Pivetta et al. (2019); m: Pugliese et al. (2021); * this work. Modified from González et al. (2017).

et al., 2000). However, some previous ages (Rb–Sr, K–Ar) suggest an older age for the beginning of this magmatism, recently confirmed by U–Pb zircon ages (Núñez et al., 1975; Cortés, 1981; Genovese, 1995; Busteros et al., 1998; Strazzere et al., 2017, 2019; Pavón Pivetta et al., 2019; Pugliese et al., 2021). Fig. 1 shows the outcrop's distribution and published radiometric ages of the Mesozoic magmatism in the eastern North Patagonian Massif. In this work, we combine the mentioned dating-methods to constrain the age of a single volcanic event in the Lower Jurassic Marifil Volcanic Complex, and to improve the understanding of its evolution in the Valcheta - Aguada Cecilio area (Figs. 1 and 2). Petrography, DRX and whole-rock chemical data were used to approach a thorough interpretation of the geochronology and thermochronology data.

Considering the wide range of ages covered by all the volcanic centres of the extensive Marifil Volcanic Complex (Fig. 1), we believe that their integration for regional interpretations should be performed very carefully, after the individual analysis of each centre in particular. Therefore, the results and interpretations of this study are exclusive for the sampled pyroclastic bed and the effusive centre where it belongs.

However, considering that the construction of the Marifil Volcanic Complex occurred through a succession of recurrent single volcanic events over time, some general assumptions can be drawn for the acidic Jurassic magmatism in the North Patagonian Massif.

2. Geological setting

The geology of the Valcheta-Aguada Cecilio area (Fig. 2) consists of four main lithological groups: 1) Paleozoic rocks, 2) Early Jurassic igneous and sedimentary rocks, 3) Late Cretaceous to Paleogene sedimentary and volcanic rocks, and 4) Neogene to Quaternary deposits.

2.1. Paleozoic rocks

Paleozoic rocks comprise metamorphic, igneous, and sedimentary rocks widely distributed in the area (Fig. 2).

The Nahuel Niyeu Formation (Caminos, 1983) is a low-metamorphic grade unit integrated mainly by metasandstones and phyllites with minor intercalations of metaigneous rocks (Chernicoff and Caminos, 1996; Giacosa, 1999; Caminos et al., 2001; Greco et al., 2015, 2017). Sedimentary and igneous protoliths of the Nahuel Niyeu Formation yield Cambrian maximum depositional and crystallization ages (Pankhurst et al., 2006; Rapalini et al., 2013; Greco et al., 2015, 2017). Between Valcheta and Aguada Cecilio, the Nahuel Niyeu Formation exhibits a complex structure, probably developed during three evolutionary stages: early and late Paleozoic, and post-Early Jurassic to pre-Late Cretaceous (Giacosa, 1999; Greco et al., 2015, 2017, 2018).

Muscovite-biotite-bearing granitic plutons and dykes, and tonalitic plutons intrude the Nahuel Niyeu Formation in the area (Núñez et al., 1975; Caminos et al., 2001; López de Luchi et al., 2008; Gozalvez, 2009a, 2010; Rapalini et al., 2013). Ar–Ar and K–Ar cooling ages range from Ordovician to Silurian (López de Luchi et al., 2008; Gozalvez, 2009a; Rapalini et al., 2013; Martínez Dopico et al., 2017), as previously suggested by Núñez et al. (1975) and Caminos et al. (2001).

A deformed sedimentary sequence assigned to the Silurian-Devonian Sierra Grande Formation unconformably covers the Nahuel Niyeu Formation (Sesana, 1968; Methol and Sesana, 1972; Núñez et al., 1975; Chernicoff and Caminos, 1996; Caminos et al., 2001; von Gosen, 2003). It is composed of arenites, gravelly sandstones, conglomerates, siltstones, and claystones.

Finally, Permian granitoids of the Navarrete Plutonic Complex intrude the Nahuel Niyeu Formation (Caminos, 1983; Caminos et al., 2001; Pankhurst et al., 2006; Gozalvez, 2009b).

2.2. Lower Jurassic igneous and sedimentary rocks

The Marifil Volcanic Complex (Malvicini and Llambías, 1974; -nom. transl.- Cortés, 1981; Giacosa, 1993) crops out in wide areas of the eastern North Patagonian Massif (Kay et al., 1989; Rapela and

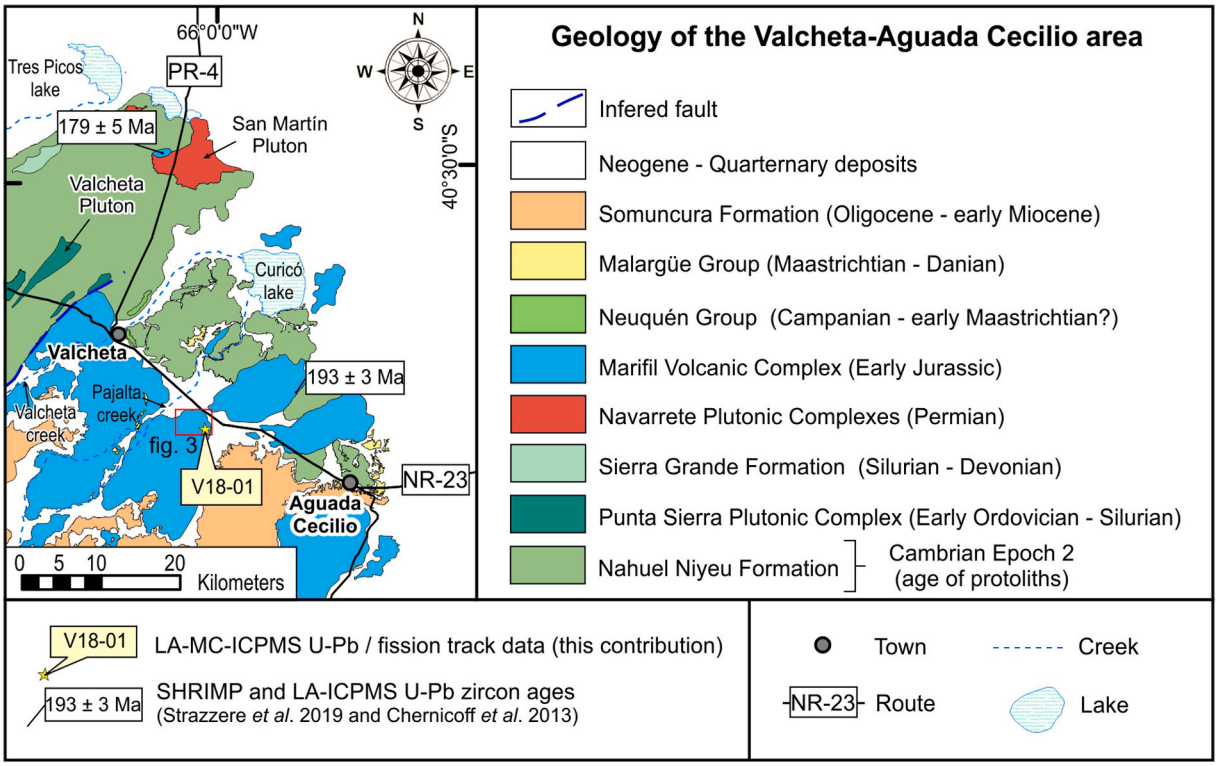

Fig. 2. Geological map of the Valcheta-Aguada Cecilio area, based and modified after Greco et al. (2015). U–Pb data from Chernicoff et al. (2017) and Strazzere et al. (2019) are indicated as well as the location of the sample V18-01.

Pankhurst, 1993; Pankhurst and Rapela, 1995; Aragón et al., 1996; Pankhurst et al., 1998; Caminos et al., 2001; Márquez et al., 2010, 2011; González et al., 2017; Pavón Pivetta et al., 2019) and represent the Lower Jurassic igneous and sedimentary rocks from the Valcheta - Aguada Cecilio area. In this area, basal strata of the Marifil Volcanic Complex include the Puesto Piris Formation consisting of conglomerates, gravelly sandstones, sandstones, tuffs, and limestones that unconformably cover the Nahuel Niyeu Formation (Núñez et al., 1975; Strazzere et al., 2019). The age of this unit has been attributed to the Triassic - Early Jurassic (Núñez et al., 1975; Caminos et al., 2001; Martínez et al., 2001). However, new geochronological data support a possible Early Jurassic age for this unit (Strazzere et al., 2019).

An acidic volcanic sequence composed of rhyodacitic to rhyolitic ignimbrites and lava flows; and minor trachytic lava flows, tuffs, conglomerates, and sandstones, covers both the Puesto Piris and the Nahuel Niyeu formations (Nuñez et al., 1975; Caminos, 2001; Martinez et al., 2001). The acidic volcanic sequence represents the upper section of the Marifil Volcanic Complex (González et al., 2017). Trachytic and rhyolitic to rhyodacitic dykes and domes intruding the acidic volcanic sequence and the Paleozoic rocks, are also considered as part of the Marifil Volcanic Complex (Caminos et al., 2001; Márquez et al., 2011; Chernicoff et al., 2017; Strazzere et al., 2019).

The Marifil Volcanic Complex shows homoclinal structures as well as faults and gentle to open folds in the area (Núñez et al., 1975; Martínez et al., 2001; Chernicoff et al., 2017; Greco et al., 2018, 2021a, 2021b; Strazzere et al., 2019). These structures are equivalent to those affecting the Nahuel Niyeu Formation and developed during a Toarciam and pre-Late Cretaceous contractional stage (Greco et al., 2018, 2021c).

The age of the Marifil Volcanic Complex in the Valcheta-Aguada Cecilio area has been constrained on the basis of fossiliferous content and K–Ar cooling ages of a volcano-sedimentary sequence covering the Puesto Piris Formation (Núñez et al., 1975). These authors considered the acidic volcanic rocks of the sequence as formed during the Early to Middle Jurassic. Rb–Sr, K–Ar and Ar–Ar -whole rock and mineral-radiometric ages have constrained the duration of the Marifil magmatism in the North Patagonian Massif between Late Triassic and Late Jurassic (Fig. 1; Núñez et al., 1975; Vallés, 1978; Cortés, 1981; Haller, 1981; Rapela and Pankhurst, 1993; Genovese, 1995; Pankhurst and Rapela, 1995; Busteros et al., 1998; Féraud et al., 1999; Franchi et al., 2001). SHRIMP and LA-ICP-MS U–Pb zircon ages obtained from sub-volcanic and lava bodies in this unit range between 193.4 Ma and 179 Ma (Fig. 1; Sinemurian to Toarcian, Chernicoff et al., 2017; Strazzere et al., 2017, 2019; Pavón Pivetta et al., 2019; Pugliese et al., 2021). Based on the ages of the rocks of the Marifil Volcanic Complex, they might be grouped in the V1 (188-178 Ma) and V2 (172-162 Ma) eruptive stages proposed by Pankhurst et al. (2000) for the Jurassic Chon Aike Silicic Large Igneous Province. Older ages have been considered as representative of a V0 eruptive stage (Pavón Pivetta et al., 2019).

2.3. Upper Cretaceous to paleogene sedimentary and volcanic rocks

Upper Cretaceous to Cenozoic sedimentary and volcanic rocks are represented by the Neuquén and Malargüe Groups and the Somuncura Formation, which cover both the Paleozoic and the Early Jurassic geological units (Caminos et al., 2001; Martínez et al., 2001). In the study area, the Neuquén (Campanian-early Maastrichtian?) and the Malargüe (Maastrichtian-Danian) groups comprise sedimentary fossiliferous beds of continental and marine origin respectively (Caminos et al., 2001; Martínez et al., 2001). The Oligocene to lower Miocene Somuncura Formation covers wide areas of the North Patagonian Massif and represents mafic volcanic fields (Ardolino, 1981; Ardolino and Franchi, 1993; Kay et al., 2007).

2.4. Neogene-quaternary deposits

Neogene to Quaternary deposits cover the previously mentioned units. They comprise continental sedimentary rocks and alluvial/colluvial deposits widely developed in the area (Caminos et al., 2001; Martínez et al., 2001).

3. Materials and methods

Field mapping and sampling were performed in the study area using satellite imagery in a portable android device with a GPS sensor. A single ignimbrite bed from the Marifil Volcanic Complex was sampled collecting 10 kg of two whole-rock samples and one pumice concentrate of ~2 kg (sample V18-01, 40°47′10″S; 66°2′18″W, Figs. 2 and 3).

Petrographic thin sections were performed by the Petroctomy Laboratory at Instituto de Investigaciones en Paleobiología y Geología (Rio Negro-Argentina).

Sample preparation and DRX analysis for alteration assessment have been carried out in the DRX laboratory at Instituto de Investigaciones en Paleobiología y Geología. Detailed information about these techniques and diffractometer specifications are available in the supplementary data.

A sample from the pumice fraction was used to concentrate zircons to obtain U–Pb ages. Besides, whole-rock samples were used to concentrate apatites and zircons to perform: (1) apatite fission track (AFT), and (2) double dating of zircon-crystals by applying zircon fission track (ZFT) and U–Pb on the same zircon-grains. Apatite and Zircon Fission Track (AFT and ZFT, respectively) are low-temperature thermochronometers that provide the time of cooling of a rock sample through a specific range of temperature. Both methods are based on the analysis and counting of narrow zones of damage called “fission tracks” that are formed in the crystal lattice as a result of the spontaneous fission decay of the ^{238}U (Price and Walker, 1963; Fleischer et al., 1975). The length of the fission tracks depends on temperature, and significant track shortening occurs within thermal ranges of 60–120 °C for apatites and 200–300 °C for zircons, both known as Partial Annealing Zone (PAZ, Gleadow and Fitzgerald, 1987; Tagami, 2005). A long residence in or above the PAZ results in the thermal recovery of the crystal lattice and the erasing of the fission tracks (Fleischer et al., 1975). Below these temperature ranges, the fission tracks start to be retained in the crystals (Laslett et al., 1987; Brandon et al., 1998; Ketcham et al., 1999). The closure temperature (Tc) of both FT isotopic systems that controls the loss or retention of radiogenic decay products, are 240 ± 20 °C for ZFT and 100 ± 10 °C for AFT (Dodson, 1973; Laslett et al., 1987; Brandon et al., 1998). Fission Track analytical data are available in the supplementary data.

Zircons from the pumice fraction were analysed in the laboratories at Centro de Pesquisas em Geocronologia e Geoquímica Isotópica of São Paulo (CPGeo). Fission track and U–Pb techniques applied on the whole-rock sample were performed at La.Te Andes S.A. laboratory (Salta, Argentina). U–Pb results were analysed and processed with Isoplot/Ex software (Ludwig, 2008) and IsoplotR (Vermeesch, 2018). In addition, density and radial plots were produced in order to visualize and analyse the dispersion of the results (Vermeesch, 2009, 2012). Fission track results were processed with Trackkey software (Dunkl, 2002) and displayed with density and radial plot as well. Macroscopic and microscopic descriptions of the ignimbrite were carried out during field-work and then under a petrographic microscope. Analitical data and further details about U–Pb and FT methodologies, can be found in the supplementary data.

Pyroclastic rocks usually contain lithic fragments with zircon crystals resulting in diverse populations of grain-ages in the whole-rock sample. This dispersion of grain-ages likely conceals the original crystallization age of the volcaniclastic unit. Consequently, zircon crystals from both flattened pumice fragments (*fiamme*) and a whole-rock sample were concentrated separately, and results were compared in detail to distinguish the potential inherited signals. As the pumice fragments in pyroclastic rocks are considered juvenile glassy components (McPhie et al., 1993), the zircon crystals contained in them could be thought as formed roughly near the age of the volcanic burst. Likewise, the U–Pb

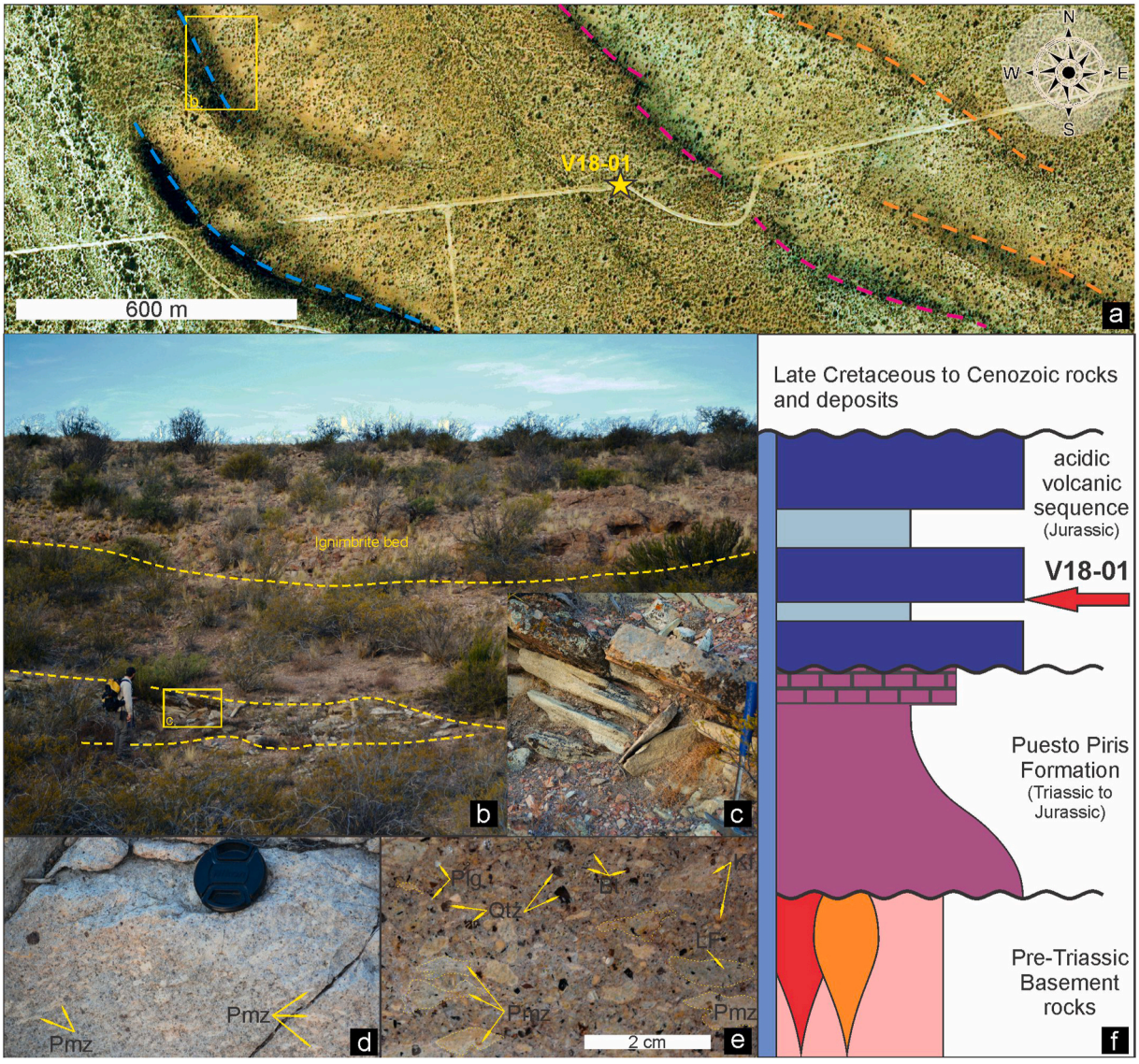

Fig. 3. Field photographs from the study area showing their spatial location. a. satellite image from the area where the sample V18-01 was obtained, the location is marked in Fig. 2. Coloured dot-lines demark different pyroclastic beds; b. photograph from a typical Marifil Volcanic Complex outcrop where there is a thin, fine stratified sequence under a massive ignimbrite bed; c. detail in the stratified sequence from b.; d. outcrop photograph of the ignimbrite from sample V18-01; e. polished section of a hand specimen from sample V18-01 showing the horizontal alignment of *fiamme* defining the eutaxitic texture and the major components (Pmz = flattened pumice fragment (*fiamme*); Qtz = quartz crystaloclast; Kf = K-feldspar crystaloclast; LT = lithoclast; Plg = plagioclase crystaloclast; Bt = biotite crystaloclast); f. schematic stratigraphic column showing the relation between lithostratigraphic units in the area and the position of the V18-01 sample. The Marifil Volcanic Complex is divided into 3 units in the column, the Puesto Piris Formation at the base in purple color, the acidic volcanic sequence (including pyroclastic beds in dark blue and epiclastic beds in light blue) and the intrusive bodies which are indicated as a vertical blue bar in the left.

crystallization age of those zircon crystals might reflect the age of the volcanic event represented by the pyroclastic bed as well. However, the analytical uncertainty of the U–Pb method could be larger than the interval of a single volcanic event. In the case of the Fission Track method, cooling ages might have different meanings depending on the rock-type analysed. For sedimentary rocks, the fission tracks retained by its zircon and apatite crystals record the thermal history of their respective provenances, rather than post-depositional cooling events, when it has not been subjected to temperatures higher or within the PAZ after its deposition. In the case of volcanic units, fission tracks would reflect a high-rates, rapid volcanic cooling with crystallization and cooling ages overlapped. However, volcaniclastic units merit to be processed and analysed carefully. The presence of derived components from the volcanic apparatus and/or incorporated during the transportation can disguise the original crystallization age of the pyroclastic bed, leading to discrepancies between crystallization and cooling ages.

Considering this, this work discusses the significance of the U–Pb zircon ages obtained from the pumice fragments and the whole-rock sample. Moreover, a detailed comparison between U–Pb ages and AFT and ZFT cooling ages is performed in order to reconstruct the evolution of the ignimbrite bed.

4. Results

4.1. Petrography

The samples analysed in this work were collected from a pyroclastic sequence with minor epiclastic intercalations located 15 km SE of Valcheta (Figs. 2 and 3). This pyroclastic sequence has been assigned to the Marifil Volcanic Complex because of its texture, composition and stratigraphic position (Nuñez et al., 1975; Caminos et al., 2001). The sample corresponds to a light grey pyroclastic rock with fragmental

texture characterized by the presence of lithic, crystal and pumice (vitric) fragments. Flat pumice fragments (*fiamme*) define a eutaxitic texture (Figs. 3 and 4). The *fiamme* are white to light pink and partly conserve their micro-vesicular texture. They reach 3 cm long and 5 mm thick. The glass is devitrified and some *fiamme* show a concentric structure of devitrification with relatively large, euhedral quartz and feldspar crystals in the centre, and an outer zone with fibrous radial crystals of the same minerals (Fig. 4a).

Embayed bipyramidal quartz, perthitic K-feldspar, zoned plagioclase and biotite are common crystaloclasts (Fig. 4b, c, d and e). They present euhedral to anhedral shapes and their size ranges from 4 mm to 0.5 mm. Limpid, non-twinned outer rims are common in plagioclase and K-feldspar crystaloclast. Clusters of large euhedral plagioclase crystals with sieve texture are common (Fig. 4d and e). Opaque minerals are disseminated and some present cubic and octahedral shapes. As the sample reacts to a hand magnet, a large fraction of the opaque crystals might correspond to magnetite.

The lithoclasts are mainly volcanic and pyroclastic, with trachytic and rhyolitic composition. Small and scarce fragments from low grade metamorphic rocks have been recognized in hand specimens. The size of lithoclast ranges between 2 cm and 2 mm.

K-feldspar crystals are slightly altered to hydromicas (possibly illite), biotite crystals are oxidized and the glass of the pumice fragments and matrix is completely devitrified. The matrix of the rocks is composed of a fine mosaic of quartz and feldspars, probably produced by devitrification, where no juvenile glassy components could be recognized (Fig. 4b, c, d and e). Chlorite and epidote with traces of calcite are scarce alteration minerals. They appear as small aggregates infilling cavities.

The grain size distribution comprises mostly ash and lapilli. According to its grain size and crystal composition, the rock could be

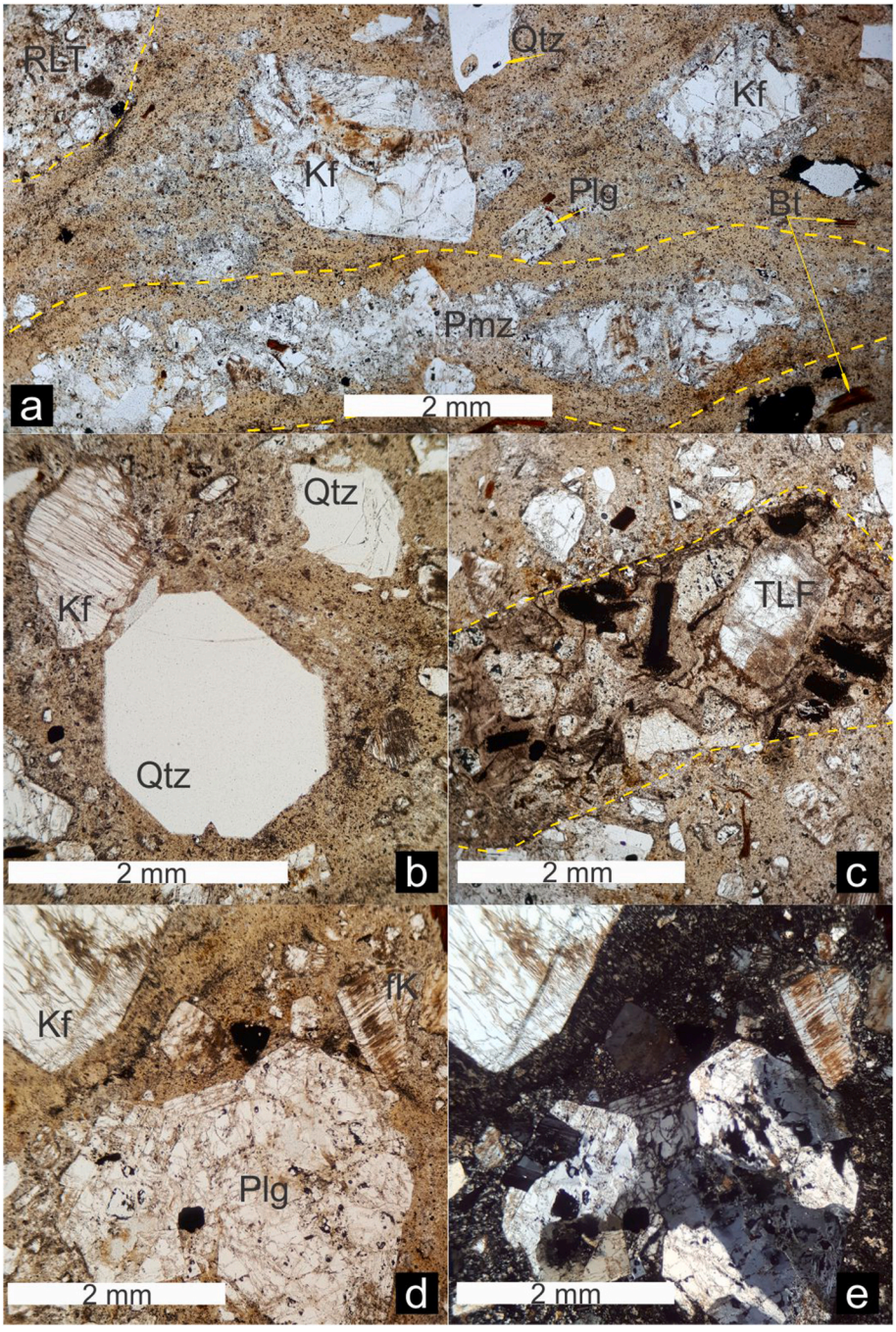

Fig. 4. Detailed photograph from the analysed ignimbrite (V18-01). a. plane-polarized light photomicrograph showing the general aspect of the ignimbrite (RLT = rhyolitic lithoclast); b. plane-polarized light photomicrograph showing in the centre a euhedral bipyramidal quartz (Qtz) crystaloclast, in the right superior corner a euhedral quartz crystaloclast and in the left an anhedral, altered pertitic K-feldspar (Kf) crystaloclast; c. plane-polarized light photomicrograph showing a trachytic lithoclast (TLF); d. plane-polarized light photomicrograph showing a lithoclast composed of plagioclase crystals (Plg); e. cross-polarized light photomicrograph from d., sieve texture can be recognized in some plagioclase crystals; the matrix of the rock forms a fine mosaic of quartz and feldspar as product of devitrification. (Bt = biotite).

classified as a rhyolitic lapilli tuff. Considering the pyroclastic nature of the rock, its eutaxitic texture, the size heterogeneity of the fragments and the high participation of juvenile material, we interpret this rock as an ignimbrite, product of a pyroclastic density current deposit.

4.2. Assessment of the Marifil Volcanic Complex alteration

During petrographic characterization, some signs of alteration were observed in the analysed rhyolitic ignimbrite. In order to evaluate the influence of alteration processes over geochronologic and thermocronologic results, we performed DRX analyses (whole rock and clay fraction from sample V18-01) to complete the characterization of the alteration paragenesis. Then, a regional alteration analysis is proposed based on the chemical information available on the rhyolitic rocks of the Marifil Volcanic Complex.

4.2.1. DRX analysis

The application of DRX analysis on sample V18-01 permitted us to recognise and separate clay mineral phases. Following the Rietveld Refinement Method (Rietveld, 1969; see supplementary data for further details), 7.45% of clay minerals were recognized for the whole sample. The clay fraction is composed of Illite (70%) and smectite (30%). The illite peak is clearly distinguished from the smectites peak either in bulk-rock, oriented and glycolated analyses. There is no evidence of mixed layer clay minerals (illite/smectite) peak.

Clays from the smectite group are common products of volcanic materials weathering. Illite type clays are formed from Al-rich silicates under high-pH weathering or hydrothermal alteration conditions. As a generalization, illite forms at higher temperatures than smectite. During the burial of epiclastic rocks, the temperature increment produces a gradual transformation of smectite into illite (Tardy et al., 1987; Pollastro, 1993).

Four diagenetic zones have been defined on the basis of mineralogical changes in acidic pyroclastic rocks as a product of thermal increment during burial (after Iijima, 1978 in Tsolis-Katagas and Katagas, 1990 and Gifkins et al., 2005). Clays from the smectite group prevail in shallow Zone 1 and tend to disappear in deeper zones. Illite becomes dominant in Zone 3 under higher temperature and pressure conditions. The coexistence of illite and smectite as individual minerals (no mixed layer) could be interpreted as formed during different events. The illite might represent an early stage, probably linked to a synvolcanic diagenesis (Gifkins et al., 2005), because thermal conditions to its formation could produce the disappearance of smectite in the rock. Therefore, smectite could have been formed later, during the exhumation of the sequence.

4.2.2. Chemical approach

Considering the age and composition of the Marifil Volcanic Complex, and its belonging to the Chon Aike Silicic Large Igneous Province, a possible alteration process might be evaluated following the ideas of Páez et al. (2010). Our evaluation is based on a geochemical database of 65 published analyses from rhyolitic rock-sample of the Marifil Volcanic Complex (geochemical data from Giacosa, 1993; Pankhurst and Rapela, 1995; Busteros et al., 1998; Márquez et al., 2011; González et al., 2016; Pavón Pivetta et al., 2019; Navarrete et al., 2019).

The "Alteration Box Plot" (Large et al., 2001; Gifkins et al., 2005), based on Ishikawa alteration index (AI) and chlorite-carbonate-pyrite index (CCPI), can also be constructed with the available data to evaluate possible alteration processes in the rhyolites from the Marifil Volcanic Complex. The "Alteration Box Plot" is a way of discriminating geochemical trends due to diagenetic alteration from those due to hydrothermal alteration (Large et al., 2001 and references therein; Fig. 5a). The samples from the Marifil Volcanic Complex are scattered following a tendency compatible with an early diagenetic alteration trend. However, some samples show a hydrothermal alteration signature, probably related to hydrothermal deposits hosted and related to Marifil Volcanic Complex rocks (e.g., Gozalvez, 2010; Dill et al., 2013, 2016; Pavón Pivetta et al., 2019).

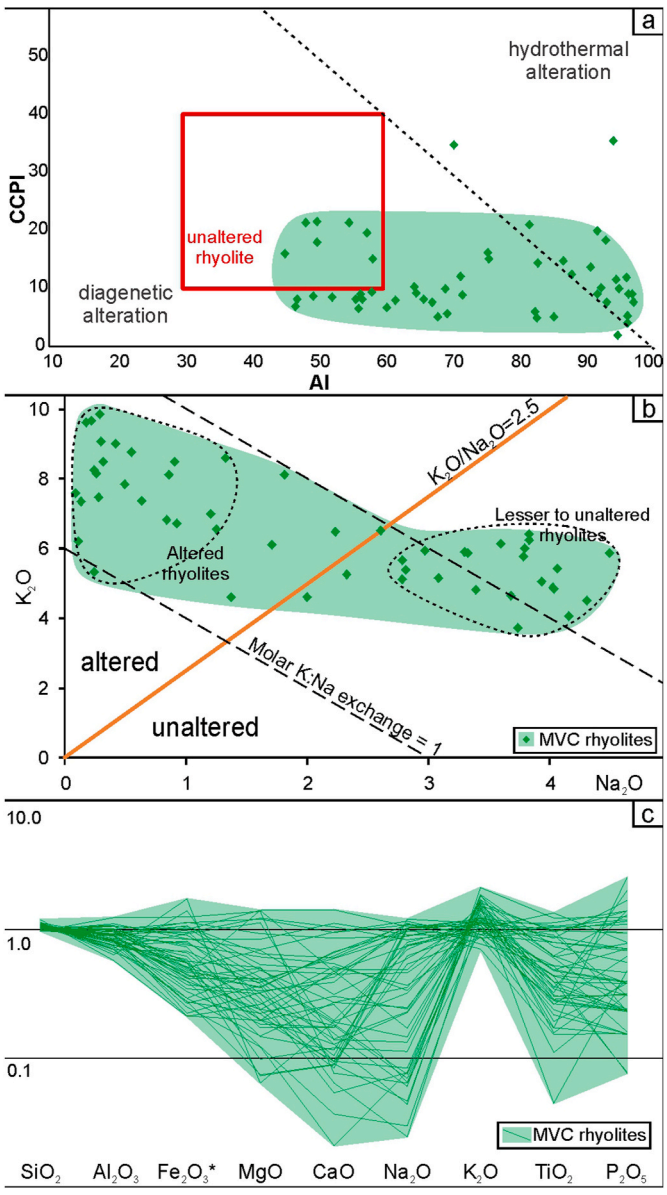

Fig. 5. Boxplot for alteration assessment. a. "Alteration Box Plot" (after Large et al., 2001; Gifkins et al., 2005) where the samples from the Marifil Volcanic Complex follow an early diagenetic alteration trend; b. K2O/Na2O ratio plot after Páez et al. (2010), this diagram discriminated two groups of samples, altered rhyolites and lesser or unaltered rhyolites; c. multi-elemental normalization diagram using unaltered rhyolites composition as normalization values.

The K_2O/Na_2O ratio as crucial to discriminate altered rhyolites (Páez et al., 2010). In Fig. 5b this ratio allows the recognition of two groups of samples, altered rhyolites and slightly or unaltered rhyolites. Using the average chemical composition from the unaltered rhyolites (from the Alteration Box Plot), a multi-elemental normalization diagram is proposed in Fig. 5c. This diagram presents significant additions of K_2O against loss in MgO, CaO, Na_2O and P_2O_5. Similar elemental patterns have been noticed in regional scale potassic metasomatism (Páez et al., 2010). According to these authors, this process only affects rocks with silica contents over 68 wt%.

In volcanogenic rocks, the principal change due to diagenesis is the formation of alkali-rich silicate minerals such as clays at the expense of feldspars and glass (Large et al., 2001). The presence of clay minerals has been confirmed by petrography and DRX analysis of the V18-01 sample.

This sample could be included as part of the diagenetic alteration trend of the rhyolitic samples from the Marifil Volcanic Complex.

4.3. U–Pb zircon ages

4.3.1. Pumice fragments

Around 100 igneous zircon crystals with euhedral prismatic habit were separated from the pumice fragments. Their aspect ratios range between 1:2 and 1:4 and the length of their major axis varies between 100 and 250 μm. The crystals are mostly limpid with scarce fiuid inclusions. Fifty-nine crystals were mounted in epoxy resin to perform CL images and posterior U–Pb analysis. They presented a typical igneous morphology with a high A index and a low to medium T index (classes I, R1-4; Pupin, 1980) with oscillatory zonation, although some crystals describe sector zonation (Fig. 6a). In some grains, obliteration of primary zonation can be recognized as homogeneous grey areas or as complete rims around the crystals (e.g., Fig. 6a grain 3.1, Fig. 6c grain G29). These images are compatible with partial metamictisation of the zircon lattice (Ault et al., 2018). The spots to be analysed were selected using the previously mentioned images considering the internal structure and the fracturing degree of the crystals (McLaren et al., 1994).

Thirty-six zircon crystals were analysed by the LA-ICP-MS U–Pb method. The Th/U ratio of the crystals ranges between 0.35 and 2.63 (Table 1 in supplementary data). Individual ages range between 151 and 218 Ma. The oscillatory zoning structure and the Th/U ratio (>0.1) of the analysed zircons are typical of magmatic crystals. Twenty of the thirty-six analysed zircons were rejected because of high ^{206}Pb of common origin and analytic problems. The sixteen remaining spots allow us to calculate a Concordia age of 184.4 ± 1.1 Ma using the Tera-Wasserbug diagram (MSWD = 0.013; Fig. 6b; Table 1 in supplementary data).

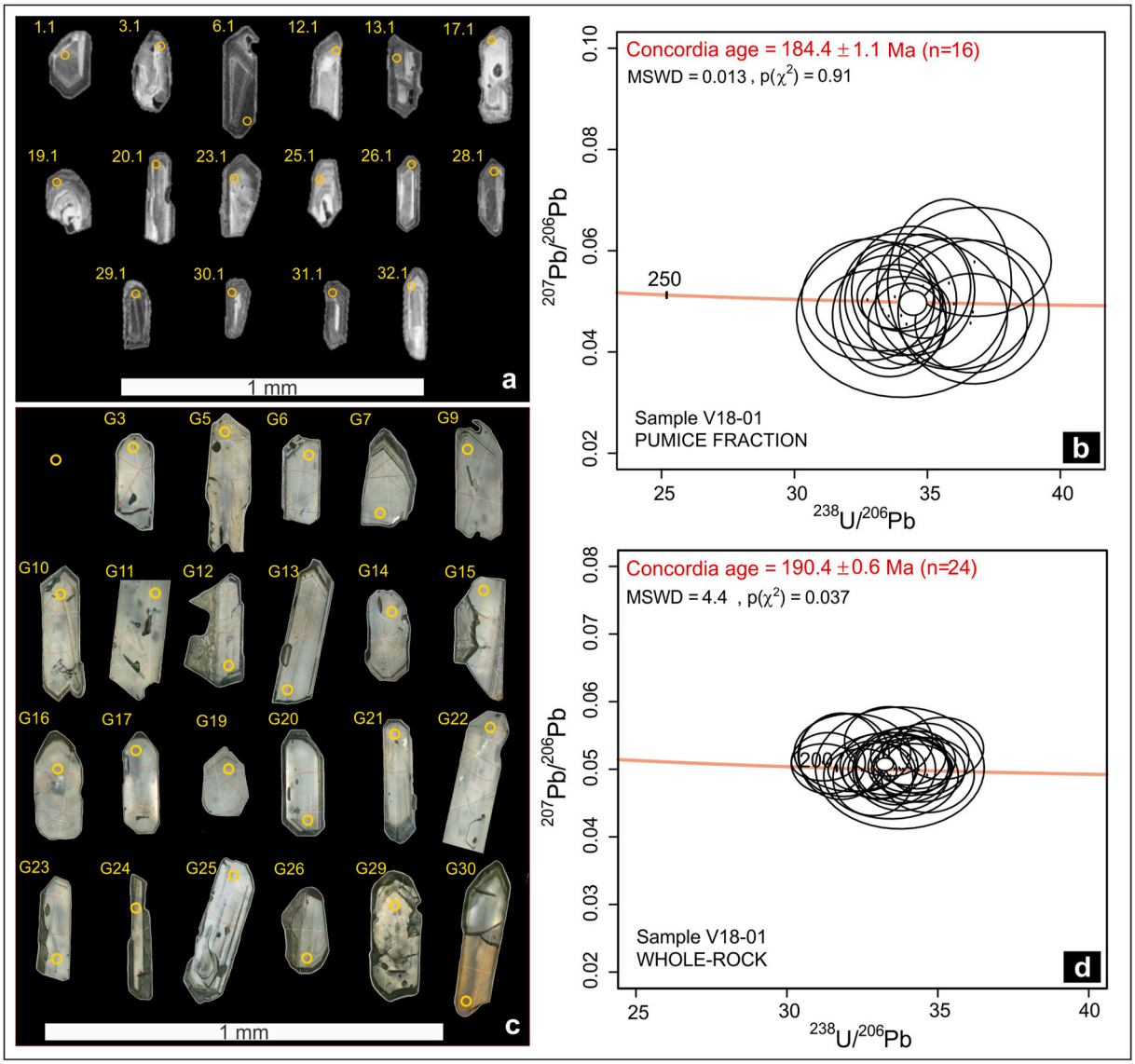

Fig. 6. Zircon crystals from sample V18-01 used for the estimation of each Concordia age and Tera–Wasserburg Concordia diagrams developed through IsoplotR Software (Vermeesch, 2018). Error ellipses are shown as 2σ. Concordance results and statistical indexes of MSWD (Mean Square Weighted Deviation) and P(x2) (probability of obtaining x2-value for n degrees of freedom, where n = number of crystals) are also specified. Values of MSWD<1 are indicative of underdispersed results, with an overestimation of the analytical uncertainties; and P(x2)>0.05 is indicative of a homogenous population. a. Zircon crystals of the pumice fraction sample used for the estimation of the Concordia age, with the location of the ablation-spots; b. Results of the pumice fraction of V18-01 obtained at Centro de Pesquisas em Geocronologia e Geoquímica Isotópica, São Paulo - Brazil (CPGeo); c. Zircon crystals of the whole-rock sample used for the estimation of the concordia age, with the location of the ablation-spots; d. Results of the whole-rock sample of V18-01 obtained in La.Te. Andes S.A. at Vaqueros, Salta, Argentina.

4.3.2. Whole-rock

The same zircon crystals used to perform ZFT methodology were analysed with LA-ICP-MS. These grains describe uniform morphologies with unaltered euhedral zircon crystals, with well-developed tetragonal pyramid and prism faces (Fig. 6c). The Th/U ratio of the crystals varies between 0.79 and 2.60 (Table 2 in supplementary data). Individual ages range between 177 and 203 Ma. Twenty-four zircon ages allow us to calculate a Concordia age of 190.4 ± 0.6 Ma using Tera-Wasserbug diagram (MSWD = 4.4; Fig. 6d; Table 2 in supplementary data).

4.4. Apatite and zircon fission track (AFT - ZFT)

Thirty-five apatite crystals from sample V18-01 yielded an Early Jurassic central cooling age of 179.1 ± 13.5 Ma (Toarcian) (Fig. 7a; Tables 3 and 4 in supplementary data). The grain-age distribution has a P(x^2)>5% consistent with a single population of ages (Galbraith, 1981; Green, 1981). Mean values from kinetic parameters of confined track lengths and Dpar are 14.1 ± 1.2 μm and 1.7 μm respectively, both with a uniform distribution consistent with the presence of a single population of ages (Fig. 7a; Table 5 in supplementary data).

Thirty zircon crystals from the same sample yielded an Early Jurassic central cooling age of 172.5 ± 8.1 Ma (Aalenian) (Fig. 7b; Tables 6 and 7 in supplementary data). The sample passed the Chi square test (P(x^2)≫ 5%) indicative of the presence of a unique population of ages.

The absence of overdispersed grain-ages in both AFT and ZFT results, and their suitability for using a central age, is reflected in the low dispersion of their radial plots (Fig. 7) and in the presence of single peaks on their density and frequency distributions. Analytic results are presented in the supplementary data (Tables 3–8).

Finally, the morphological analysis of the crystals dated with fission track techniques revealed the presence of uniform morphologies, with unaltered euhedral to subhedral apatite crystals and unaltered euhedral zircon crystals. Both apatite and zircon crystals have prism and bipyramid as euhedral crystalline forms (Fig. 8). These characteristics likely evidence the existence of a unique morphological group, which is consistent with the uniform distribution of their grain-ages related to single AFT and ZFT central ages in each case.

5. Discussion

While a single volcanic event might take place in a few days or years, volcanic centres of large magmatic provinces might have a lifetime of 10^5 to 10^7 years. This scenario of a maintained magmatism over time requires a sustained and localized magma flux at rates higher than the average to support long-live magmatic systems (Cashman et al., 2017 and reference therein). High-silica magma systems are examples of long-lasting magmatic complexes. The evolution of high-silica magmas at relatively low-temperature might include diverse processes like

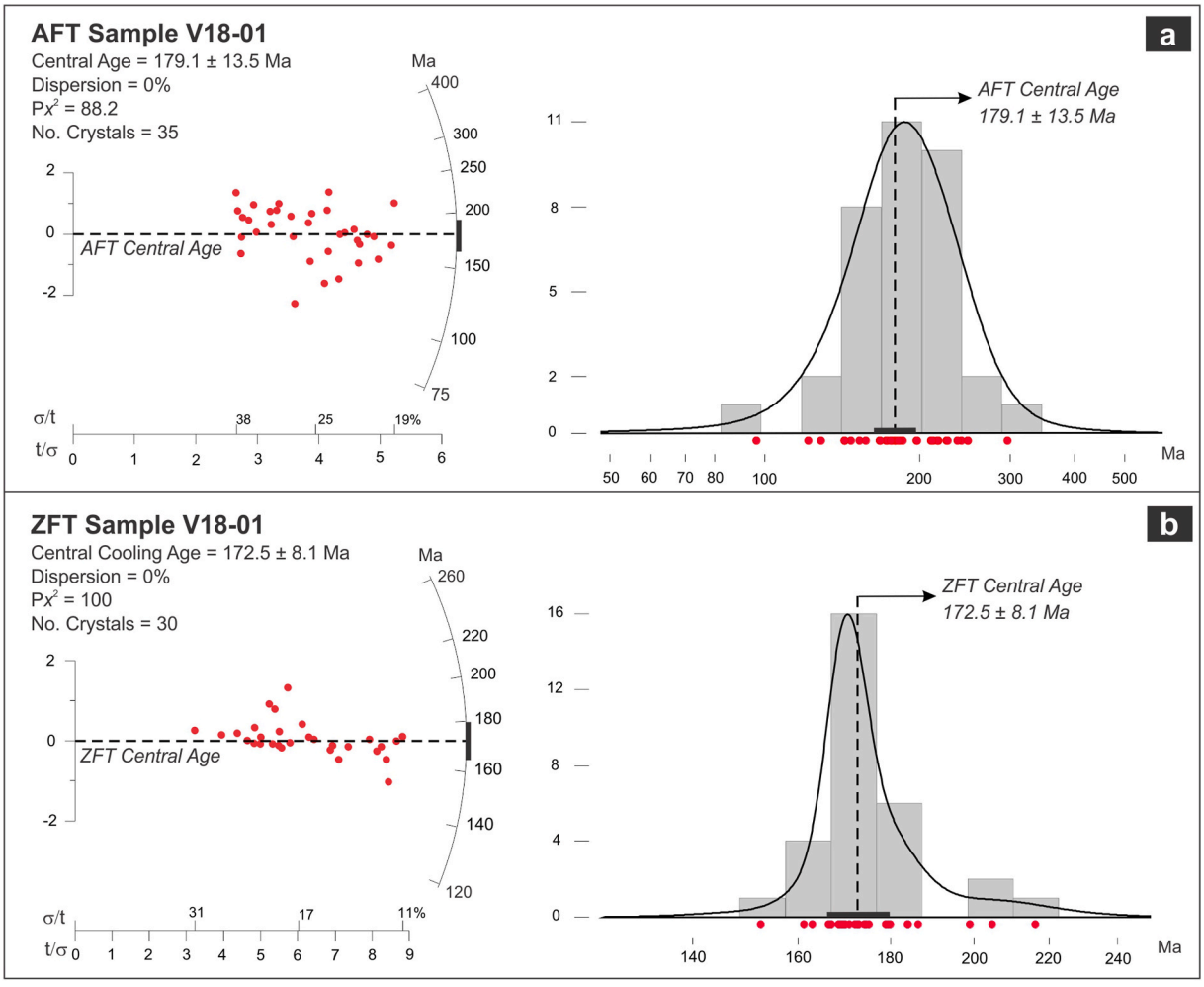

Fig. 7. Apatite (a) and zircon (b) fission track ages from sample V18-01. Fission track data is displayed by two different graphical devices: left-radial plot of single grain ages; right- Kernel density estimate (black curve) with histogram (light grey rectangles), both made using Density Plotter software intended for the visualization of detrital age distributions (Vermeesch, 2012). ZFT and AFT central ages are depicted with a dashed black line, and their range of analytical uncertainty with a black bar next to the time axis. Grain-ages are depicted with small red circles.

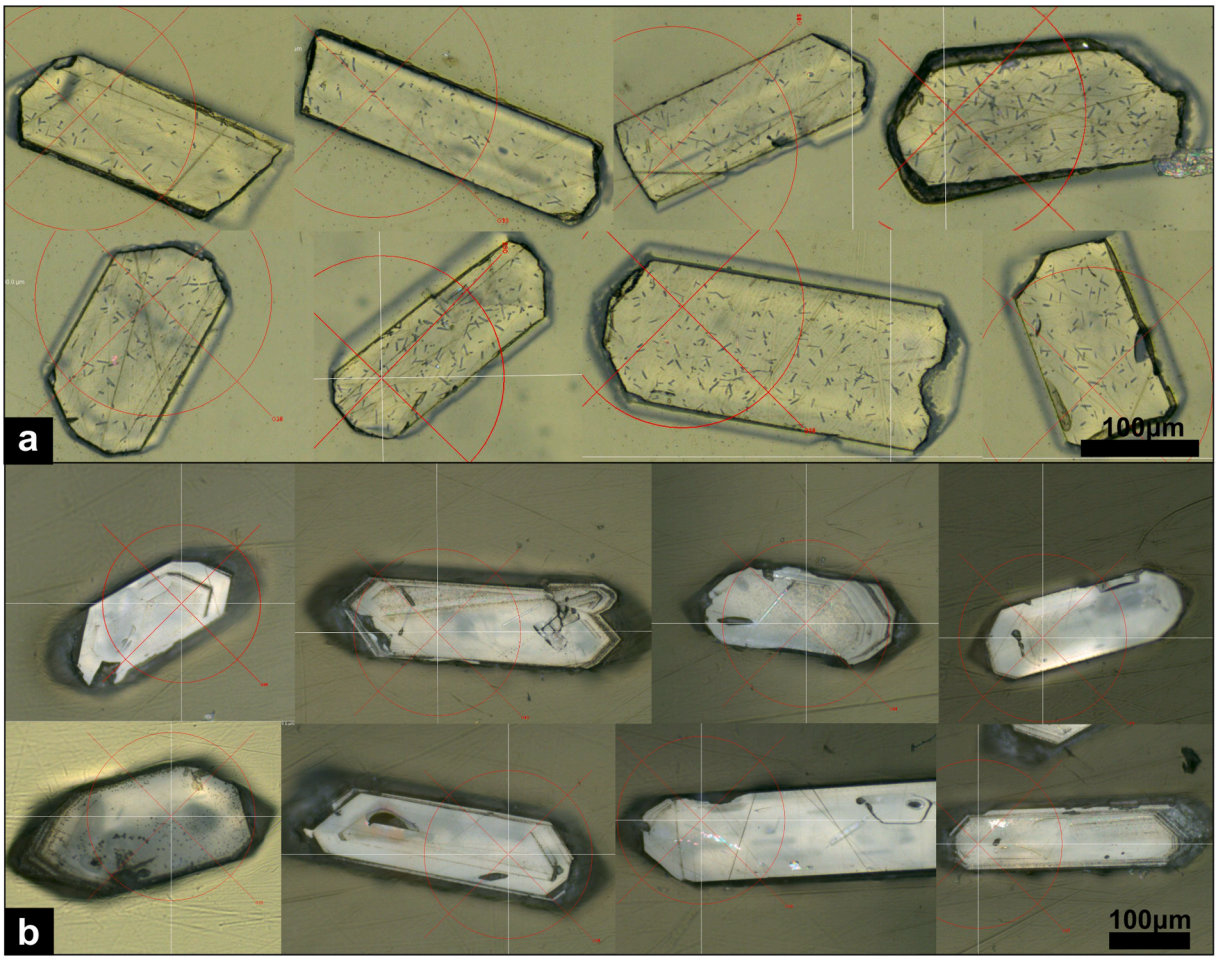

Fig. 8. Examples of the apatites (a) and zircon crystals (b) dated by fission track methodology. Zircon crystals describe uniform unaltered euhedral morphologies, and apatites euhedral to subhedral, both with well-developed crystalline forms and well-formed tetragonal prism faces. Photographs taken with Zeiss AXIO Imager Z2m binocular microscope, through TrackWorks Autoscan Software.

crystallization and remelt, or they could just remain as crystal mushes over such extensive periods (Hawkesworth et al., 2004).

In the following section, we attempt to evaluate and discuss the significance of the different ages obtained considering the geological context of the Jurassic magmatism in the North Patagonian Massif and the analysed ignimbrite in particular.

5.1. Analysis of results

5.1.1. U–Pb ages

U–Pb dating in zircon crystals of cohesive magmatic rocks helps to estimate the time scales of magma differentiation and crustal residence because of its resistance to recycling (e.g., Glazner et al., 2004; Hawkesworth et al., 2004; Gelman et al., 2013; Cooper, 2015; Kern et al., 2016). Although zircon data suggest magmatic differentiation time scales of 1^3 to $>10^5$ years, the internal structure of a single zircon crystal could include an inherited core related to older crystallization stages, or to preceding magmatism. Conversely, zircon outer layers crystallize near the time of eruption (Stelten et al., 2015). In pyroclastic rocks, the inherited signal of older fragments not related to the volcanic event tends to be significant (McCormack et al., 2009). Moreover, cogenetic rock-fragments might be easily incorporated during the eruption, creating a dispersion of ages that masks the actual age of volcanism. The inheritance in pyroclastic rocks introduces a complexity to assess the age of the involved processes (Jagodzinski, 1998). Dating juvenile materials, such as pumice fragments, seems to be the most accurate way to date the eruption and deposition of these materials but, there is still the uncertainty about the origin of the pumice fraction. Could these fractions belong to a preceding eruption and be included as lithic fragments in a younger pyroclastic deposit? Is it possible to differentiate inherited pumice from juvenile ones? In the last case, when composition is almost identical and alteration (e.g. devitrification) obscures the characteristics of the material, the recognition of inherited or juvenile features might be infeasible. In this case, a detailed analysis of grain-ages distribution would help to shed light on this issue.

From the same ignimbrite rock unit, we obtained two different zircon samples, pumice and whole-rock. For the first one, we determined a Concordia age of 184.4 ± 1.1 Ma. We consider this age as the main crystallization age represented by the dated zircon crystals. Besides the Concordia age, the five youngest crystals, with individual ages between 177 and 173 Ma, represent a minor population of 175.2 Ma. However, 3 grains of this younger population evidence a percentage of discordance higher than 5%. The existence of this young population with different degrees of concordance and the recognition of partial metamictisation in some zircon grains might be related to a variable Pb loss and rejuvenation of the U–Pb isotopic system in the affected grains (Mezger and Krogstad, 1997; Compston, 2001; Hay and Dempster, 2009).

For the whole-rock sample a Concordia age of 190.4 ± 0.6 Ma was obtained using the concordant zircon crystals. As the whole-rock sample probably includes inherited zircons, as can be thought from the presence of lithic fragments, we consider this age as a mixed age without geological meaning. Nevertheless, three age populations can be recognized using the unmix tool from Isoplot: (1) 201.2 Ma, (2) 192.3 Ma, and (3) 186.2 Ma. The latter is close to the main crystallization age obtained

from the pumice fraction zircons.

In Fig. 9, box and radial plots integrate all the concordant zircon crystals from sample V18-01. In the box plot (Fig. 9a), three groups of grains can be easily recognized. The central group includes the majority of grains representing an age ca. 185 Ma. This age is in good agreement with the main crystallization age (Concordia age of pumice fragments zircons) and the youngest population age from the whole-rock sample. Both extremes of the grain-age distribution in the plot include few crystals. While the oldest grains can be considered as inherited from lithic fragments, the youngest ones could represent Pb-loss during post-depositional and/or diagenetic events. This will be considered again after discussing the fission track ages.

According to the morphology and the concordance degree of the results, the analysed zircons are magmatic in origin (sections 4.3.1 and 4.3.2, Tables 1 and 2 in supplementary information). According to their ages, they can be enclosed in the first event of the Chon Aike magmatism (V1 sensu Pankhurst et al., 2000) although the younger zircon crystals have ages between the V1 and V2 events defined by those authors. The obtained U–Pb ages spread along a 25 Ma range, probably representing inheritance from multiple volcanic events in north-eastern Patagonia during the Early Jurassic. Fragments from Paleozoic rocks (see section 2.1) are scarce so its contribution to zircon populations was not reflected in our analyses. Inherited Late Triassic ages were obtained from some grains in the whole rock-sample, probably associated to a widespread Triassic magmatism recognized west of the study area by Caminos et al. (2001). From age inheritance and petrographic analysis, we infer that the analysed ignimbrite was formed during explosive, mainly acidic, volcanism implanted in a vast volcanic field. The older magmatic products were the foundational substrate, and they were similar in composition to posterior eruptive materials. The existence of large Jurassic eruptive centres in north-eastern Patagonia associated with the Chon Aike Igneous Province has been proposed by Ciciarelli (1990), Aragón et al. (1996) and Márquez et al. (2011).

5.1.2. Fission track ages

Fission Track ages span a range of time between 165 and 190 Ma, central ages are 179.1 ± 13.5 Ma for AFT and 172.5 ± 8.1 Ma for ZFT. This wide variation is attributed to the analytical uncertainty of both fission track methods, which compared to U–Pb grain-ages error results in a significant span of probability (Fig. 10). Nevertheless, both FT ages overlap considering their range of analytical uncertainty, thus reflecting the same rapid cooling episode (Fig. 10). This rapid cooling is consistent with the confined track lengths uniform distribution measured on the analysed apatite crystals and their mean length of 14.1 ± 1.2 μm, which is close to the initial length of the tracks when they originate (16.3 μm). This means that they were rapidly cooled with not enough time to be shortened (Fig. 11, based on Table 8 in supplementary data).

The convergence between both FT ages, plus their equivalence to U–Pb ages, reflect a unique and rapid cooling episode of the ignimbrite bed. For assessing such inference, and considering that both fission track techniques were applied on the whole-rock sample, a re-estimation of both FT central ages can be performed by filtering those FT grain-ages older than the U–Pb main crystallization age (184.4 ± 1.1 Ma, obtained from the pumice fraction), assuming that those crystals are inherited detrital components that do not belong to the pumice fraction, with a thermal history unrelated to the crystallization of the ignimbrite, and might affect the resulting age. Only one apatite-grain and no zircon-grain (considering their analytical errors) yielded a cooling-age older than the main Concordia U–Pb crystallization age. Therefore, both re-estimated central ages (AFT: 177.1 ± 13.4 Ma for n = 34; ZFT: 172.5 ± 8.1 Ma for n = 30) are almost the same as the original ones (see Supplementary Material for further details). The results of this test demonstrate that both fission track ages, AFT and ZFT, are not affected by inherited grains and they can be considered as a reflection of a single thermal event probably occurred after eruption and deposition of the ignimbrite.

The Fission Track central ages are consistent with the Concordia U–Pb age of the pumice fraction (184.4 ± 1.1 Ma). In this sense, if the

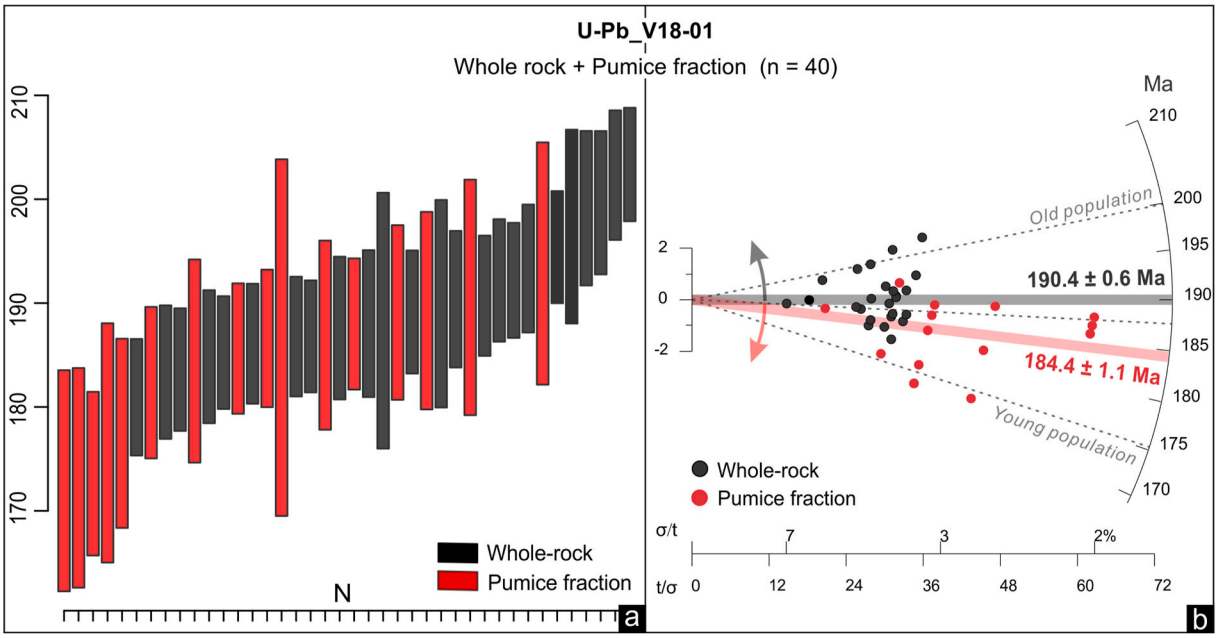

Fig. 9. Age diagrams confectioned using all the analysed zircon crystals (pumice fractions and whole-rock). a. Box plot for U–Pb data of sample V18-01, developed through IsoplotR Software (Vermeesch, 2018). Boxes correspond to the 206/238U–Pb age of each dated zircon-crystal, and boxes' heights represent their 2σ error. Note the two-tailed S-shaped distribution, where the whole-rock data tends to older ages, whereas pumice fraction data tends to younger ages. This pattern could evidence potential Pb loss content due to post-depositional hydrothermal effects in the region, and/or the presence of older inherited zircon-grains in the whole-rock sample; b. Concordant U–Pb single grain ages of sample V18-01 displayed in a radial plot using Radial Plotter software intended for the visualization of detrital age distributions (Vermeesch, 2009). Concordia ages are depicted in red (pumice fraction) and black (whole-rock). Note the tendency of pumice fraction to young grain-ages, and whole-rock to old grain-ages. Both tendencies are well-depicted by the two extreme populations identified by the software.

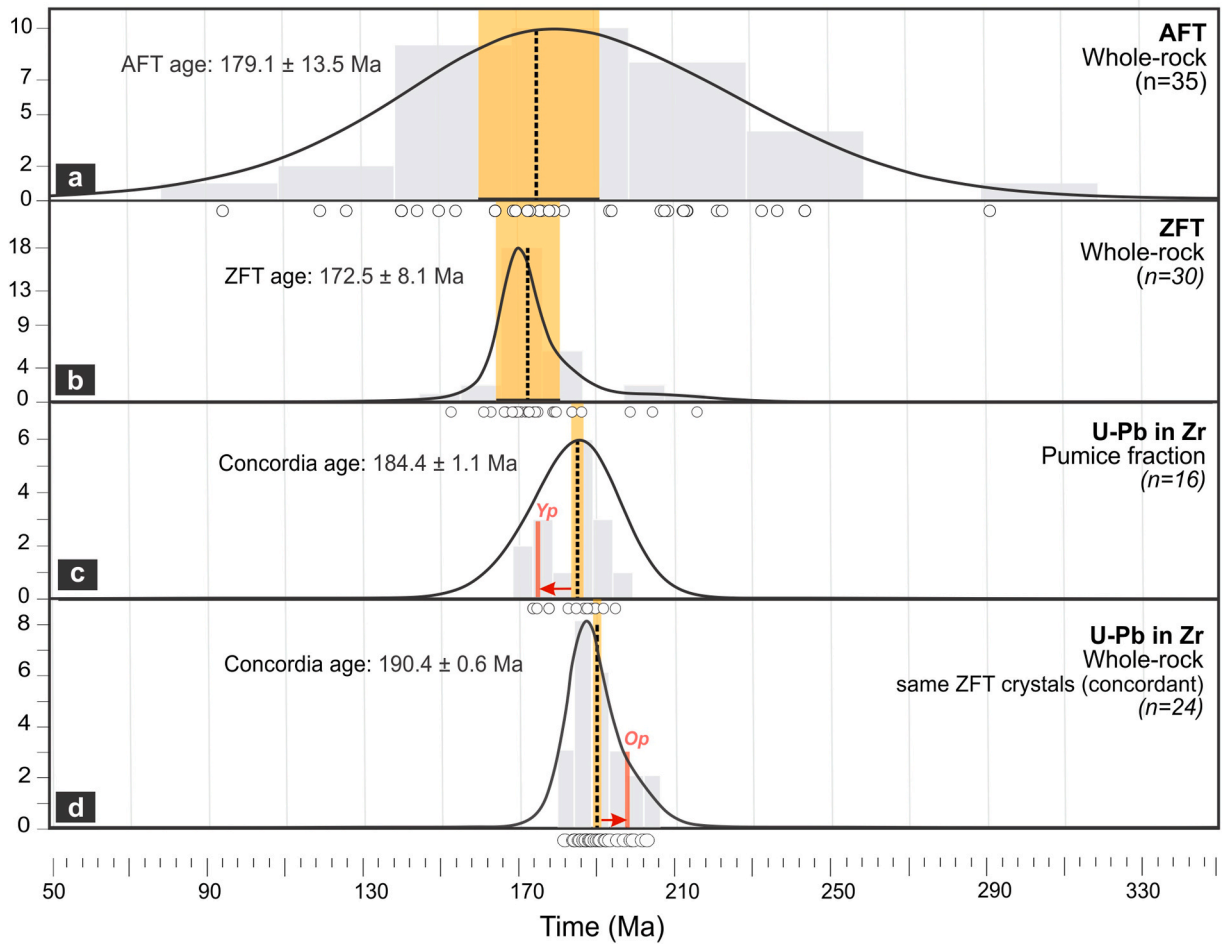

Fig. 10. Comparison between AFT, ZFT and U–Pb grain-ages represented with Kernel density estimate (black curve) and histograms (light grey rectangles), both made using Density Plotter software (Vermeesch, 2012). U–Pb crystallization age (including only concordant ages) and FT central cooling ages are depicted with a dashed black line, and their range of analytical uncertainty with a yellow area and black bar above the time axis. Grain-ages are depicted with small white circles. (a) AFT ages obtained on whole-rock sample, (b) ZFT ages performed on whole-rock sample, (c) U–Pb ages from pumice fraction, (d) U–Pb ages calculated on the same zircon dated with ZFT technique. The tendency to young zircon-ages for the pumice fraction and to old grain-ages for the whole-rock sample is represented by both the young population (Yp) and old population (Op) respectively, estimated by the Radial Plot of Figure x and indicated with red lines in each case.

closure temperatures of each isotopic system and the ages with their errors are considered, then the ignimbrite would have cooled below 240 ± 20 °C/100 ± 10 °C (Tc for ZFT and AFT respectively) in an interval of ~ 6–12 Ma. This tight gap between fission track and U–Pb ages, appreciable in the plots of Fig. 10, could reflect: (i) the time between the crystallization of zircons in the pumice fraction and its deposition and cooling after eruption, caused by a potential protracted pre-eruptive residence of the crystals in the magma reservoir; or (ii) a slight rejuvenation of fission track ages due to post-depositional processes, responsible for maintaining the high temperatures until the ultimate cooling of the ignimbrite bed. The second scenario would be the most suitable considering the diagenetic alteration process affecting the rocks of the Marifil Volcanic Complex, assessed from whole rock chemistry and recognized in sample V18-01 by petrography and the presence of illite in DRX analyses (see section 4.2). Consequently, a synvolcanic diagenetic stage (Gifkins et al., 2005) might have occurred as a product of the combination of the thermal anomaly linked to the emplacement of the voluminous Marifil magmatism, and the immediate covering of the pyroclastic sequence. As a result of this diagenetic process, the temperature of the FT systems could have remained above the PAZ after the eruption until later cooling. Additionally, the resetting of isotopic systems from Paleozoic rocks in surrounding areas has been attributed to the influence of the Jurassic magmatism ((Aragón et al., 1999; Martínez Dopico et al., 2016).

The ZFT and AFT central ages imply that the analysed rock has never been subjected to temperatures above their Tc, either within their PAZ (60–120 °C for apatites and 200–300 °C for zircons) for more than 10 Ma after the Aalenian. This is in good agreement with the Jurassic tectonic setting in North Patagonian Massif, which does not imply substantial burial depths. The depth of the largest Jurassic depocentres in the Sierra Grande area has been estimated at no more than 1.8 km using gravimetric data (Gregori et al., 2013). Moreover, the total thickness of cretaceous sediments and Neogene basaltic plateau together is less than 200 m (Caminos et al., 2001; Martínez et al., 2001). To reach the mentionated thermal conditions in a depth <2 km, a normal geothermal gradient would not be enough. If we consider hypothetical burial depths of 1.8 km the geothermal gradient required to erase the fission tracks would be between 33.3 °C/Km and 66.7 °C/Km, for at least 10 Ma. The lack of geothermal gradient measurements on Mesozoic units in North Patagonian Massif does not allow us to confirm this idea.

5.1.3. *Integration of results*

Rocks from the Marifil Volcanic Complex have been dated using different methodologies as K–Ar, Rb–Sr, Ar–Ar and U–Pb. However, the nature of the dated rock is missing in most of the previously published works, and when it is mentioned, the age corresponds to magmatic bodies as domes, dykes, or lava flows. (Fig. 1 and references therein). To the best of our knowledge, the presented in this work are the first U–Pb

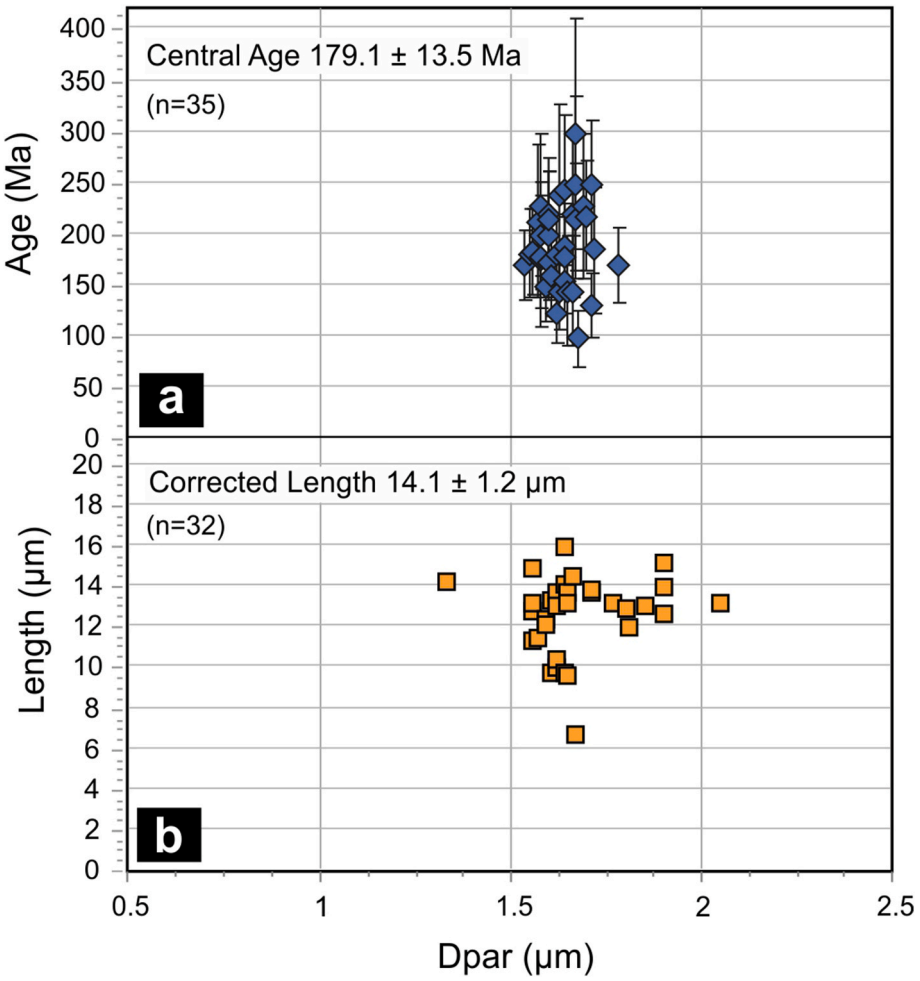

Fig. 11. (a) Grain-ages vs. Dpar of 35 apatite crystals; compared with (b) Kinetic parameters of Dpar vs. Confined track lengths of 32 apatite crystals, both from sample V18-01.

zircon, AFT and ZFT ages for an ignimbrite of the Marifil Volcanic Complex.

The analysed ignimbrite has a strong volcanic inheritance revealed by the presence of volcanic lithic fragments and by the older peak of zircon-ages from the whole-rock fraction. This inheritance likely belongs to cogenetic magmatic and pyroclastic precursors from the same effusive centre, evidenced by the ages and morphologies of the analysed zircon crystals. Most likely sources are magmatic bodies in the surroundings of the study area yielding U–Pb zircon ages in the range of the inherited peak from the whole-rock fraction (Fig. 1; Strazzere et al., 2017, 2019). Although further provenances are also plausible, seem less probable.

The Concordia age calculated in section 4.3 considers only the juvenile component of the rock (pumice-fraction zircons). Likewise, the main peak of probability for both pumice and whole-rock zircons (which includes 75% of the analysed crystals) is close to the Concordia age. The inheritance and the youngest fraction only represent the 25% of the whole analysed zircon grains, 12.5% each.

The youngest fraction has a particular relevance, since it could be considered as the closest to the eruption in terms of time. However, as was previously mentioned, there are some evidences suggesting partial Pb loss, which could explain the rejuvenation of the U–Pb system and the slightly-high discordance in some of the analysed crystals (Compston, 2001). Pb-loss in zircon might be induced by incipient weathering, fluid circulation, and low-grade metamorphism (Black, 1987; Mezger and Krogstad, 1997; Hay and Dempster, 2009, and reference therein). Some of the previously mentioned processes might take place during diagenesis. Petrology, whole-rock chemistry and DRX analysis suggest the existence of a diagenetic process affecting the studied rock. Likewise, partial metamictisation of the crystalline lattice has been considered as key-factor for Pb loss in zircon (Mezger and Krogstad, 1997; Hay and Dempster, 2009) and evidence of it has been recognized in some of the dated zircon crystals. Metamictised zircons may be partly annealed at temperatures below 200 °C (Nasdala et al., 2001). This temperature is close to the PAZ for ZTF, and this may suggest that damage in zircon will be repaired at similar low temperatures (Hay and Dempster, 2009). This coincidence between annealing temperatures could explain the closeness between the age of the young zircon population and the FT ages.

Taking into account the previous discussion, the nature of the rock and the geological context for its formation we consider the Concordia age from pumice fraction (184.4 Ma) the most reliable to estimate the age of eruption. However, the younger peak of probability for the whole-rock fraction (*ca.* 186 Ma) should not be dismiss considering a possible rejuvenation of the U–Pb system in zircon by Pb loss. Further analysis involving a larger number of crystals from the same ignimbrite and/or new data on other rock-beds from the same eruptive centre could confirm or dismiss our interpretations.

6. Conclusions and final considerations

We consider the U–Pb Concordia age of 184.4 Ma obtained from pumice zircons of the Marifil Volcanic Complex ignimbrite as the age of the pyroclastic eruption and deposition of the bed. This age is slightly older than fission track cooling ages obtained from the whole-rock sample, of 179.1 ± 13.5 Ma (AFT) and 172.5 ± 8.1 Ma (ZFT). Both

cooling ages are interpreted as a consequence of posterior diagenetic changes. Considering only the U–Pb ages in zircons available for the Marifil Volcanic Complex in the study area, the Jurassic volcanism of the study area would be restricted between 193.4 ± 3.1 Ma and 179 ± 5 Ma (Chernicoff et al., 2017; Strazzere et al., 2019; this contribution). However, the evidence of thermal effects as diagenetic processes, and the existence of hydrothermal deposits hosted and related to the Jurassic magmatism in this area, would suggest the continuation of the Marifil magmatism until ~170 Ma. In this area of the North Patagonian Massif, we recognized a single eruptive event as part of a large, long-lasting acidic magmatic system.

Fission track ages reveal that the Marifil Volcanic Complex ignimbrite did not reach burial depths greater than ~3.33 ± 0.3 km; or it would not have remained more than ~2 km for more than 10 Ma. A normal thermal gradient of 30 °C/km could be inferred for the eastern North Patagonian Massif during early Jurassic since there is no reset of fission tracks. Moreover, non-reset fission track ages evidence that a thermal quietude has prevailed in this area since Aalenian times.

Declaration of competing interest

The authors declare that they have no known competing financial interests or personal relationships that could have appeared to influence the work reported in this paper.

Acknowledgments

The authors would like to especially thank Coco Piris and Norma Piris and the people of Valcheta and Aguada Cecilio for always giving us their help and support during field work. Thanks are also extended to Dr. A. Folguera (editor) and anonymous reviewers, whose suggestions have significantly improved this study.

Financial support for this study was provided by Universidad Nacional de Río Negro (PI UNRN 40-A-535, PI-UNRN-40-A-621, PI-UNRN-40-A-865 and PI-UNRN-40-A-914), and the Agencia Nacional de Promoción Cientifica y Tecnologica (PICT 1090–2017 and PICT 0825–2018).

Appendix A. Supplementary data

Supplementary data to this article can be found online at https://doi.org/10.1016/j.jsames.2021.103688.

References

Aragón, E., Dalla Salda, L., Varela, R., Benialgo, A., 1999. Jurassic resetted ages of Gonzalito SEDEX deposit, northeastern Patagonia. II South American Symposium on Isotope Geology, Actas. Córdoba, Argentina, pp. 7–10.

Aragón, E., Rodriguez, A.M.I., Benialgo, A., 1996. A calderas field at the Marifil Formation, new volcanogenic interpretation, Norpatagonian Massif, Argentina. J. S. Am. Earth Sci. 9, 321–328.

Ardolino, A., 1981. El vulcanismo Cenozoico del borde suroriental de la meseta de Somún Curá. In: VIII Congreso Geológico Argentino, pp. 7–23. Actas.

Ardolino, A., Franchi, M., 1993. El vulcanismo cenozoico de la Meseta de Somún curá, Río Negro Y Chubut: XII Congreso Geológico ArgentinoActas, vol. 4, pp. 225–235.

Ault, Alexis K., Guenthner, William R., Moser, Amy C., Miller, Gifford H., Refsnider, Kurt A., 2018. Zircon grain selection reveals (de)coupled metamictization, radiation damage, and He diffusivity. Chem. Geol. 490, 1–12.

Black, L.P., 1987. Recent pb loss in zircon: a natural or laboratory-Induced phenomenon? Chem. Geol. 65, 25–33.

Brandon, M.T., Roden-Tice, M.K., Garver, J.I., 1998. Late cenozoic exhumation of the cascadia accretionary wedge in the olympic mountains, northwest Washington state. GSA Bulletin 110, 985–1009.

Busteros, A., Giacosa, R., Lema, H., 1998. Hoja Geológica 4166-IV, Sierra Grande, Provincia de Río Negro. Servicio Geológico Minero Argentino, Buenos Aires, p. 75.

Caminos, R., 1983. Descripción geológica de las Hojas 39g, Cerro Tapiluke y 39h. In: Chipauquil, provincia de Río Negro. Servicio Geológico Nacional, Buenos Aires.

Caminos, R., Chernicoff, C.J., Fauqué, L., Franchi, M., 2001. Hoja Geológica 4166-I, Valcheta, provincia de Río Negro: Buenos Aires. Instituto de Geología y Recursos Minerales - Servicio Geológico Minero Argentino, p. 73.

Cashman, K.V., Sparks, R.S.J., Blundy, J.D., 2017. Vertically extensive and unstable magmatic systems: a unified view of igneous processes. Science 355, eaag3055.

Chernicoff, C.J., Caminos, R., 1996. Estructura y relaciones estratigráficas de la Formación Nahuel Niyeu, macizo nordpatagónico oriental. Provincia de Río Negro: Rev. Asoc. Geol. Argent. 51, 201–212.

Chernicoff, C.J., Gozalvez, M.R., Santos, J.O., Mc Naughton, N.J., 2017. Edad U-Pb SHRIMP en circones y caracterización de la Riolita Punta del Agua, sector centro-oriental de la provincia de Río Negro, Argentina: nueva evidencia de la compresión jurásica inferior en la Pataginia oriental: XX Congreso Geológico Argentino. In: Actas Simposio, vol. 15. San Miguel de Tucumán, pp. 14–15.

Ciciarelli, M.I., 1990. Análisis estructural del sector oriental del Macizo Nordpatagónico y su significado metalogenético. Provincias de Río Negro y Chubut [Ph.D. thesis]: La Plata. Universidad Nacional de La Plata, p. 178.

Compston, W., 2001. Effect of Pb loss on the ages of reference zircons QGNG and SL13, and of volcanic zircons from the early devonian merrions and turondale formations, new south wales. Aust. J. Earth Sci. 48, 797–803.

Cooper, K.M., 2015. Timescales of Crustal Magma Reservoir Processes: Insights from U-Series Crystal Ages, vol. 422. Geological Society, London, Special Publications, pp. 141–174.

Cortés, J., 1981. El substrato precretácico del extremo noreste de la Provincia del Chubut. Rev. Asoc. Geol. Argent. 36, 217–235.

Dill, G.H., Garrido, M.M., Melcher, F., Gomez, M.C., Weber, B., Luna, L.I., Bahr, A., 2013. Sulfidic and non-sulfidic indium mineralization of the epithermal Au–Cu–Zn–Pb–Ag deposit San Roque (Provincia Rio Negro, SE Argentina) — with special reference to the "indium window" in zinc sulfide. Ore Geol. Rev. 51, 103–128. https://doi.org/10.1016/j.oregeorev.2012.12.005.

Dill, G.H., Luna, L.I., Nolte, N., Hanssen, B.T., 2016. Chemical, isotopic and mineralogical epithermal characteristics of volcanogenic fluorite deposits on the Andean Permo-Mesozoic foreland of the volcanic arc in Patagonia (Argentina). Chem. Erde 76 (2), 275–297. https://doi.org/10.1016/j.chemer.2016.03.002.

Dodson, M.H., 1973. Closure temperature in cooling geochronological and petrological systems. Contrib. Mineral. Petrol. 40, 259–274.

Dunkl, I., 2002. Trackkey: a Windows program for calculation and graphical presentation of fission track data. Comput. Geosci. 28, 3–12.

Féraud, G., Alric, V., Fornari, M., Bertrand, H., Haller, M., 1999. 40Ar/39Ar dating of the Jurassic volcanic province of Patagonia: migrating magmatism related to Gondwana break-up and subduction. Earth Planet Sci. Lett. 172, 83–96.

Fleischer, R.L., Price, P.B., Walker, R.M., Walker, R.M., 1975. Nuclear Tracks in Solids: Principles and Applications. Univ of California Press, p. 626.

Fornelli, A., Piccarreta, G., Micheletti, F., Mörner, N., 2014. In situ U-Pb dating combined with SEM imaging on zircon-an analytical bond for effective geological recontructions. In: Morner, N.-A. (Ed.), Geochronology-Methods and Case Studies: IntechOpen, pp. 109–139.

Franchi, M., A A, Remesal, M., 2001. Hoja Geológica 4166-III, Cona Niyeu, provincia de Río Negro: Buenos Aires. Instituto de Geología y Recursos Minerales - Servicio Geológico Minero Argentino, p. 83.

Galbraith, R.F., 1981. On statistical models for fission track counts. J. Int. Assoc. Math. Geol. 13, 471–478.

Gallagher, K., 2012. Transdimensional inverse thermal history modeling for quantitative thermochronology. J. Geophys. Res. Solid Earth 117.

Gelman, S.E., Gutiérrez, F.J., Bachmann, O., 2013. On the longevity of large upper crustal silicic magma reservoirs. Geology 41, 759–762.

Genovese, S., 1995. Geología y geocronología del área de la mina La Leona, departamento San Antonio, provincia de Río Negro. Dissertation: Buenos Aires. Universidad Nacional de Buenos Aires, p. 76.

Giacosa, R., 1993. El ciclo eruptivo gondwánico en el área de Sierra Pailemán, Macizo Nordpatagónico, Argentina. XII Congreso Geológico Argentino y 2 Congreso de Exploración de hidrocarburos, Mendoza, Actas, pp. 113–119.

Giacosa, R., 1999. El basamento pre-silúrico del extremo este del Macizo Nordpatagónico y del Macizo del Deseado. In: Caminos, R. (Ed.), Geología Argentina. Instituto de Geología y Recursos Minerales – SEGEMAR, Buenos Aires, pp. 118–123.

Gifkins, C., Herrmann, W., Large, R., 2005. Altered Volcanic Rocks: A Guide to Description and Interpretation. Centre for Ore Deposit Research, University of Tasmania, Australia, p. 275.

Glazner, A.F., Bartley, J.M., Coleman, D.S., Gray, W., Taylor, R.Z., 2004. Are plutons assembled over millions of years by amalgamation from small magma chambers? GSA Today (Geol. Soc. Am.) 14, 4–12.

Gleadow, A.J.W., Fitzgerald, P.G., 1987. Uplift history and structure of the Transantarctic Mountains: new evidence from fission track dating of basement apatites in the Dry Valleys area. southern Victoria Land: Earth Planet Sci. Lett. 82, 1–14.

González, S.N., Greco, G.A., González, P.D., Sato, A.M., Llambías, E.J., Varela, R., 2016. Geochemistry of a triassic dyke swarm in the north patagonian Massif, Argentina. Implications for a postorogenic event of the permian gondwanide orogeny. J. S. Am. Earth Sci. 70, 69–82.

González, S.N., Greco, G.A., Sato, A.M., González, P.D., Llambías, E.J., Díaz-Martínez, I., De Valais, S., Serra-Varela, S., 2017. Revisión estratigráfica del Complejo Volcánico Marifil. In: XX Congreso Geológico Argentino: San Miguel de Tucumán, pp. 72–77.

Gozalvez, M.R., 2009a. Petrografía y edad 40Ar/39Ar de leucogranitos peraluminosos al oeste de Valcheta: macizo Nordpatagónico (Río Negro). Rev. Asoc. Geol. Argent. 64, 285–294.

Gozalvez, M.R., 2009b. Caracterización del plutón San Martín y las mineralizaciones de wolframio asociadas, departamento Valcheta, provincia de Río Negro. Rev. Asoc. Geol. Argent. 64, 409–425.

Gozalvez, M.R., 2010. Metalogénesis asociada a la evolución magmática de las secuencias eruptivas gondwánicas en el área de Valcheta y alrededores, provincia de Río Negro [Ph.D. thesis]. Córdoba, Universidad Nacional de Córdoba, p. 202.

Greco, G.A., González, P.D., González, S.N., Sato, A.M., Basei, M.A.S., Tassinari, C.C.G., Sato, K., Varela, R., Llambías, E.J., 2015. Geology, structure and age of the Nahuel Niyeu formation in the Aguada Cecilio area, North Patagonian Massif, Argentina. J. S. Am. Earth Sci. 62, 12–32.
Greco, G.A., González, S.N., Sato, A.M., González, P.D., Basei, M.A.S., Llambías, E.J., Varela, R., 2017. The Nahuel Niyeu basin: a cambrian forearc basin in the eastern North patagonian Massif. J. S. Am. Earth Sci. 79, 111–136.
Greco, G.A., González, S.N., Giacosa, R.E., Serra-Varela, S., Melo, M., Ison, J.I., 2018. Estructuras de deformación del Paleozoico y Mesozoico en la Formación Nahuel Niyeu, basamento del este del Macizo Norpatagónico, Río Negro XVII Reunión de Tectónica, La Rioja, Resúmenes, p. 75.
Greco, G.A., González, S.N., Vera, D.R., Giacosa, R.E., 2021a. Pliegues tectónicos en el Complejo Volcánico Marifil, Este del Macizo Norpatagónico, Río Negro. XVIII Reunión de Tectónica Argentina, San Luis. Acta 46.
Greco, G.A., González, S.N., Vera, D.R., Giacosa, R.E., 2021b. El antiforme arroyo Pajalta: un pliegue mesozoico con fallas de acomodación en la Formación Nahuel Niyeu, basamento del Este del Macizo Norpatagónico, Río Negro. XVIII Reunión de Tectónica Argentina, San Luis. Acta 45.
Greco, G.A., González, S.N., Vera, D.R., Giacosa, R.E., 2021c. Contracción NO-SE del Toarciense – pre-Cretácico Tardío en el Este del Macizo Norpatagónico. XVIII Reunión de Tectónica Argentina, San Luis. Acta 47.
Green, P.F., 1981. A new look at statistics in fission-track dating. Nucl. Tracks 5, 77–86.
Gregori, D.A., Kostadinoff, J., Alvarez, G., Raniolo, A., Strazzere, L., Martínez, J.C., Barros, M., 2013. Preandean geological configuration of the eastern North patagonian Massif, Argentina. Geosci. Front. 4, 693–708.
Haller, M., 1981. Descripción geológica de la Hoja 43 h, Puerto Madryn, provincia de Chubut. Servicio Geológico Nacional, Buenos Aires.
Hawkesworth, C., George, R., Turner, S., Zellmer, G., 2004. Time scales of magmatic processes. Earth Planet Sci. Lett. 218, 1–16.
Hay, D.C., Dempster, T.J., 2009. Zircon behaviour during low-temperature metamorphism. J. Petrol. 50 (4), 571–5758 9.
Jagodzinski, E., 1998. SHRIMP U-Pb dating of ignimbrites in the pul pul rhyolite, northern territory. AGSO Res. Newsl. 28, 23–25.
Kay, S.M., Ramos, V.A., Mpodozis, C., Sruoga, P., 1989. Late paleozoic to jurassic silicic magmatism at the gondwana margin: analogy to the Middle proterozoic in north America? Geology 17, 324–328.
Kay, S.M., Ardolino, A.A., Gorring, M.L., Ramos, V.A., 2007. The Somuncura large igneous province in Patagonia: interaction of a transient mantle thermal anomaly with a subducting slab. J. Petrol. 48, 43–77.
Kern, J.M., de Silva, S.L., Schmitt, A.K., Kaiser, J.F., Iriarte, A.R., Economos, R., 2016. Geochronological imaging of an episodically constructed subvolcanic batholith: U-Pb in zircon chronochemistry of the Altiplano-Puna Volcanic Complex of the Central Andes. Geosphere 12, 1054–1077.
Ketcham, R.A., Donelick, R.A., Carlson, W.D., 1999. Variability of apatite fission-track annealing kinetics: III. Extrapolation to geological time scales: Am. Mineral. 84, 1235–1255.
Large, R.R., Gemmell, J.B., Paulick, H., Huston, D.L., 2001. The alteration box plot: a simple approach to understanding the relationship between alteration mineralogy and lithogeochemistry associated with volcanic-hosted massive sulfide deposits. Econ. Geol. 96 (5), 957–971.
Laslett, G.M., Green, P.F., Duddy, I.R., Gleadow, A.J.W., 1987. Thermal annealing of fission tracks in apatite 2. A quantitative analysis: Chem. Geol. Isot. Geosci. 65, 1–13.
López de Luchi, M.G., Wemmer, K., Rapalini, A.E., 2008. The Cooling History of the North Patagonian Massif: First Results for the Granitoids of the Valcheta Area, Río Negro, Argentina: 6th South American Symposium on Isotope Geology. San Carlos de Bariloche, Abstracts, p. 33.
Ludwig, K.R., 2008. User's Manual for Isoplot 3.6. In: A Geochronological Toolkit for Microsoft Excel, vol. 4. Berkeley Geochronology Center Special Publication, p. 77.
Malvicini, L., Llambías, E., 1974. Geología y génesis del depósito de manganeso Arroyo Verde, provincia del Chubut. V Congreso Geológico Argentino, Córdoba, Actas, pp. 185–202.
Márquez, M.J., Massaferro, G.I., Fernández, M.I., 2010. El volcanismo del complejo Marifil en Arroyo Verde, vertiente suroriental del Macizo de Somún Cura, Chubut. Rev. Asoc. Geol. Argent. 66, 314–324.
Márquez, M.J., Massaferro, G.I., Fernández, M.I., Menegatti, N., Navarrete, C.R., 2011. El centro volcánico Sierra Grande: caracterización petrográfica y geoquímica del magmatismo extensional liásico, noroeste de la Patagonia. Rev. Asoc. Geol. Argent. 68, 555–570.
Martínez Dopico, C.I., López de Luchi, M., Wemmer, K., Luppo, T., Rapalini, A.E., Buceta, G., 2017. Geochronolgy and Geochemistry of Hybrid Quartz Monzogabbro to Granodiorite Stocks of the Valcheta Plutonic Complex, North-Eastern Patagonia: XX Congreso Geológico Argentino, vol. 15. San Miguel de Tucumán, Simposio, pp. 76–78.
Martínez Dopico, Tohver, E., López de Luchi, M.G., Wemmer, K., Rapalini, A.E., Cawood, P.A., 2016. Jurassic cooling ages in Paleozoic to early Mesozoic granitoids of northeastern Patagonia: $^{40}Ar/^{40}Ar$, ^{40}K-^{40}Ar mica and U–Pb zircon evidence. International Journal of Earth Sciences. https://doi.org/10.1007/s00531-016-1430-0.
Martínez, H., Náñez, C., Lizuain, C.D.M., Turel, A., 2001. Hoja Geológica 4166-II, San Antonio Oeste, provincia de Río Negro: Buenos Aires. Instituto de Geología y Recursos Minerales - Servicio Geológico Minero Argentino, p. 32.
McCormack, K.D., Mary Gee, M.A., McNaughton, N.J., Smith, R., Fletcher, I.R., 2009. U–Pb dating of magmatic and xenocryst zircons from Mangakino ignimbrites and their correlation with detrital zircons from the Torlesse metasediments, Taupo Volcanic Zone, New Zealand. J. Volcanol. Geoth. Res. 183, 97–111.
McLaren, A.C., Gerald, J.D.F., Williams, I.S., 1994. The microstructure of zircon and its influence on the age determination from Pb/U isotopic ratios measured by ion microprobe. Geochem. Cosmochim. Acta 58, 993–1005.
McPhie, J., Doyle, M., Allen, R., 1993. Volcanic Textures: a Guide to the Interpretation of Textures in Volcanic Rocks: Australia. CODES Key Centre, University of Tasmania.
Methol, E.J., Sesana, F., 1972. Notas sobre el hallazgo de ortocuarcitas conglomerádicas en la región septentrional del Macizo Norpatagónico. Servicio Nacional Minero Geológico, Buenos Aires.
Mezger, K., Krogstad, E.J., 1997. Interpretation of discordant U-Pb zircon ages: an evaluation. J. Metamorph. Geol. 15 (1), 127–140.
Navarrete, C., Gianni, G., Encinas, A., Márquez, M., Kamerbeek, Y., Valle, M., Folguera, A., 2019. Triassic to Middle Jurassic geodynamic evolution of southwestern Gondwana: from a large flat-slab to mantle plume suction in a rollback subduction setting. Earth Sci. Rev. 194, 125–159.
Nasdala, L., Marita, W., Gerhard, V., Imer, G., Wenzel, T., Kober, B., 2001. Metamictization of natural zircon: accumulation versus thermal annealing of radioactivity-induced damage. Contrib. Mineral. Petrol. 141, 124–144.
Núñez, E., Bachmann, E.W., de, R.I., Britos, A., Franchi, M., Lizuaín, A., Sepúlveda, E., 1975. Rasgos geológicos del sector oriental del Macizo Somuncura, provincia de Río Negro, República Argentina. 2° Congreso Iberoamericano de Geología Económica, Buenos Aires, Actas, pp. 247–266.
Páez, G.N., Ruiz, R., Guido, D.M., Jovic, S.M., Schalamuk, I.B., 2010. The effects of K-metasomatism in the bahía laura volcanic complex, deseado Massif, Argentina: petrologic and metallogenic consequences. Chem. Geol. 273 (3), 300–313.
Pankhurst, R.J., Rapela, C.W., 1995. Production of Jurassic rhyolite by anatexis of the lower crust of Patagonia. Earth Planet Sci. Lett. 134, 23–36.
Pankhurst, R.J., Leat, P.T., Sruoga, P., Rapela, C.W., Márquez, M., Storey, B.C., Riley, T. R., 1998. The Chon Aike province of Patagonia and related rocks in West Antarctica: a silicic large igneous province. J. Volcanol. Geoth. Res. 81, 113–136.
Pankhurst, R.J., Riley, T.R., Fanning, C.M., Kelley, S.P., 2000. Episodic silicic volcanism in Patagonia and the antarctic peninsula: chronology of magmatism associated with the break-up of gondwana. J. Petrol. 41, 605–625.
Pankhurst, R.J., Rapela, C.W., Fanning, C.M., Márquez, M., 2006. Gondwanide continental collision and the origin of Patagonia. Earth Sci. Rev. 76, 235–257.
Pankhurst, M.J., Schaefer, B.F., Betts, P.G., 2011. Geodynamics of rapid voluminous felsic magmatism through time. Lithos 123, 92–101, 2011.
Pavón Pivetta, C., Gregori, D., Benedini, L., Garrido, M., Strazzere, L., Geraldes, M., Santos, A.C.d., Marcos, P., 2019. Contrasting tectonic settings in northern Chon Aike igneous province of Patagonia: subduction and mantle plume-related volcanism in the Marifil formation. Int. Geol. Rev. 1–27.
Pollastro, R.M., 1993. Considerations and applications of the Illite/Smectite geothermometer in hydrocarbon-bearing rocks of Miocene to Mississipian age. Clay Clay Miner. 41 (2), 119–133.
Price, P.B., Walker, R.M., 1963. Fossil tracks of charged particles in mica and the age of minerals. Journal of Geophysical Research (1896-1977 68, 4847–4862.
Pugliese, F.E., Pugliese, L.E., Dahlquist, J.A., Basei, M.A.S., Martínez Dopico, C.I., 2021. Intermediate sulfidation epithermal Pb - Zn (± Ag ± Cu ± In) and low sulfidation Au (±Pb ± Ag ± Zn) mineralization styles in the Gonzalito polymetallic mining district, North Patagonian Massif. J. S. Am. Earth Sci. https://doi.org/10.1016/j.jsames.2021.103388.
Pupin, J.P., 1980. Zircon and granite petrology. Contrib. Mineral. Petrol. 73, 207–220.
Rapalini, A.E., López de Luchi, M., Tohver, E., Cawood, P.A., 2013. The South American ancestry of the North Patagonian Massif: geochronological evidence for an autochthonous origin? Terra. Nova 25, 337–342.
Rapela, C.W., Pankhurst, R.J., 1993. El volcanismo riolítico del noreste de la Patagonia: un evento meso-jurásico de corta duración y origen profundo: XII Congreso Geológico Argentino y 2 Congreso de Exploración de Hidrocarburos, pp. 179–188. Mendoza, Actas.
Rietveld, H.M., 1969. A profile refinement method for nuclear and magnetic structures. J. Appl. Crystallogr. 2, 65–71. https://doi.org/10.1107/s0021889869006558.
Sesana, F.L., 1968. Consideraciones geológicas y petrográficas del plan Valcheta. Dirección Nacional de Geología y Minería, Buenos Aires.
Simon, J.I., Renne, P.R., Mundil, R., 2008. Implications of pre-eruptive magmatic histories of zircons for U–Pb geochronology of silicic extrusions. Earth Planet Sci. Lett. 266, 182–194.
Stelten, M.E., Cooper, K.M., Vazquez, J.A., Calvert, A.T., Glessner, J.J.G., 2015. Mechanisms and timescales of generating eruptible rhyolitic magmas at yellowstone caldera from zircon and sanidine geochronology and geochemistry. J. Petrol. 56, 1607–1642.
Storm, S., Shane, P., Schmitt, A.K., Lindsay, J.M., 2011. Contrasting punctuated zircon growth in two syn-erupted rhyolite magmas from Tarawera volcano: insights to crystal diversity in magmatic systems. Earth Planet Sci. Lett. 301, 511–520.
Strazzere, L., Gregori, D.A., Benedini, L., Marcos, P., Barros, M.V., 2017. Edad y petrografía del Complejo Volcánico Marifil en la Sierra de Pailemán, Comarca Norpatagónica, Río Negro, Argentina. In: XX Congreso Geológico Argentino: San Miguel de Tucumán, pp. 145–150.
Strazzere, L., Gregori, D.A., Benedini, L., Marcos, P., Barros, M.V., Geraldes, M.C., Pavon Pivetta, C., 2019. The Puesto Piris Formation: evidence of basin-development in the north patagonian Massif during crustal extension associated with gondwana breakup. Geosci. Front. 10, 299–314.
Tagami, T., 2005. Zircon fission-track thermochronology and applications to fault studies. Rev. Mineral. Geochem. 58, 95–122.
Tardy, Y., Duplay, J., Fritz, B., 1987. Stability Fields of Smectites and Illites as a Function of Temperature and Chemical Composition. Technical report SKB 08-20, 34pp, 0284-3757-Stockholm - Sweden.

Tsolis-Katagas, P., Katagas, C., 1990. Zeolitic diagenesis of Oligocene pyroclastic rocks of the Metaxades area, Thrace, Greece. Mineral. Mag. 54, 95–103.
Vallés, J.M., 1978. Los yacimientos de plomo "María Teresa" y " Tres Marías", ejemplos de metalogénesis mesozoica en el Macizo Norpatagónico, provincia de Río Negro. VII Congreso Geológico Argentino, Neuquén, Actas I, pp. 71–88.
Vermeesch, P., 2009. RadialPlotter: a Java application for fission track, luminescence and other radial plots. Radiat. Meas. 44, 409–410.
Vermeesch, P., 2012. On the visualisation of detrital age distributions. Chem. Geol. 312–313, 190–194.
Vermeesch, P., 2018. IsoplotR: a free and open toolbox for geochronology. Geosci. Front. 9, 1479–1493.
von Gosen, W., 2003. Thrust tectonics in the north patagonian Massif (Argentina): implications for a Patagonia plate. Tectonics 22, 1005.
Zaffarana, C.B., Lagorio, S.L., Gallastegui, G., Wörner, G., Orts, D.L., Gregori, D., Poma, S., Busteros, A., Giacosa, R., Silva Nieto, D., Ruiz González, V., Boltshauser, B., Puigdomenech Negre, C., Haller, M., 2020. Petrogenetic study of the Lonco Trapial volcanism and its comparison with the Early-Middle Jurassic magmatic units from northern Patagonia. J. S. Am. Earth Sci. 101, 102624.